Regulation of defective mitochondrial DNA accumulation and transmission in *C. elegans* by the programmed cell death and aging pathways

Sagen E. Flowers[1], Rushali Kothari[1], Yamila N. Torres Cleuren[1,2], Melissa R. Alcorn[1], Chee Kiang Ewe[1], Geneva Alok[1], Pradeep M. Joshi[1], Joel H. Rothman[1]

Affiliations:

1. Department of MCD Biology and Neuroscience Research Institute, University of California Santa Barbara, CA, USA
2. Computational Biology Unit, Institute for Informatics, University of Bergen, Norway

To whom correspondence should be addressed: joel.rothman@ucsb.edu

Keywords: heteroplasmy, uaDf5, purifying selection, programmed cell death, aging, insulin signaling

ORCiD:

SEF - 0000-0002-7818-2188

YNTC- 0000-0003-2218-7243

MRA- 0000-0001-6284-3255

CKE - 0000-0003-1973-1308

GA- 0000-0001-6257-2344

PMJ- 0000-0002-4220-0559

JHR - 0000-0002-6844-1377

Abstract

The heteroplasmic state of eukaryotic cells allows for cryptic accumulation of defective mitochondrial genomes (mtDNA). "Purifying selection" mechanisms operate to remove such dysfunctional mtDNAs. We found that pro-apoptotic regulators, including the CED-3 and CSP-1 caspases, the BH3-only protein CED-13, and PCD corpse engulfment factors, are required in *C. elegans* to attenuate germline abundance of a 3.1 kb mtDNA deletion mutation, *uaDf5*, which is normally stably maintained in heteroplasmy with wildtype mtDNA. In contrast, removal of CED-4/Apaf1 or a mutation in the CED-4-interacting prodomain of CED-3, do not increase accumulation of the defective mtDNA, suggesting induction of a non-canonical germline PCD mechanism or non-apoptotic action of the CED-13/caspase axis. We also found that the abundance of germline mtDNA^{uaDf5} reproducibly increases with age of the mothers. This effect is transmitted to the offspring of older mothers, with only partial intergenerational removal of the defective mtDNA. In mutants with elevated mtDNA^{uaDf5} levels, this removal is enhanced in older mothers, suggesting an age-dependent mechanism of mtDNA quality control. Indeed, we found that both steady-state and age-related accumulation rates of *uaDf5* are markedly decreased in long-lived, and increased in short-lived, mutants. These findings reveal that regulators of both PCD and aging are required for germline mtDNA quality control and its intergenerational transmission.

41 **Introduction**

42 Mitochondrial diseases are a group of conditions that affect mitochondrial functions in
43 up to 1 in 4,300 people [1–3]. Generally, these diseases present as dysfunction in the tissues or
44 organs with the most intensive energy demands, most commonly in muscle and the nervous
45 system [4]. Many of these diseases are attributable to mutations in the mitochondrial DNA
46 (mtDNA) or nuclear DNA (nDNA), and include those disorders with defects in mitochondrial
47 function, dynamics, or quality control, or in which there is miscommunication between the
48 mitochondria and the endoplasmic reticulum (ER) [3,5]. The progressive advancement of the
49 diseased state resulting from age-dependent accumulation of mutant mtDNA is a common trait
50 among mitochondrial diseases [6–8]. While the severity of the disease varies with the nature of
51 the mutation, the most severe phenotypes result in childhood death, as in Leigh syndrome and
52 MELAS [5,9]. As there are currently no pharmacological treatments for mitochondrial diseases, it
53 is of great importance to uncover the cellular processes that underlie the regulation of mtDNA
54 quality control.

55 As mtDNAs show high mutation rates [10–12], it is critical that cells possess mechanisms
56 to remove detrimental mtDNA alleles, a process called purifying selection [13,14]. Defects in this
57 process can result in mitochondrial diseases, allowing harmful mtDNA mutations to persist
58 through the maternal germline and subsequent generations. Processes that regulate mtDNA
59 quality control include mitochondrial fission/fusion dynamics and mitophagy [8,15–20], the
60 mitochondrial unfolded protein response (UPR^{MT}; [21–27]), and the insulin/IGF-1 signaling
61 pathway (IIS; [28,29]).

62 One potential cellular process that could be used to eliminate defective mtDNAs is the
63 culling of cells bearing mtDNA mutations by programmed cell death (PCD). The mechanisms of
64 both developmentally controlled and genotoxicity-induced PCD have been shown to be well-
65 conserved across metazoans [30], and much of the machinery that choreographs this process is
66 directed by mitochondria [31–33]. Mitochondrial-dependent processes participating in PCD
67 include permeabilization of the inner mitochondrial membrane and release of mitochondrial
68 factors that mediate transduction of intermediary events in the cell suicide program [31–33].
69 Both mitochondrial function and PCD are linked to the process of organismal aging [34]. mtDNA
70 mutations accumulate in tissues as organisms age, and it has been suggested that this
71 accumulation is a major contributor to aging [35–37].

72 The nematode *C. elegans* provides an attractive model for exploring the potential role of
73 PCD in mtDNA purifying selection. The well-described, conserved PCD regulatory pathway in *C.*
74 *elegans* functions not only to eliminate 131 somatic cells during development through a rigidly
75 stereotyped program [38], but is also activated apparently stochastically during germline
76 development, resulting in the death of >95% of nuclei that would otherwise be destined to
77 become oocytes in the mature hermaphrodite [30,39–41]. In addition to this "physiological" PCD,
78 germline nuclei that have experienced genotoxic stress are eliminated through p53-dependent
79 apoptosis, as is also the case in somatic mammalian cells [42,43]. Thus, germline PCD allows for
80 selective removal of nuclei with damaged genomes, thereby preventing intergenerational
81 transmission of defective nuclear DNA. Given the prominent role played by mitochondria in the
82 PCD process, it is conceivable that mitochondrial dysfunction could trigger PCD in the germline

83 and, as such, might similarly provide a quality control mechanism for eliminating aberrant
84 mtDNA, as seen for the nuclear genome.

85 We report here that germline mtDNA quality control in *C. elegans* is influenced by
86 regulators of both PCD and the aging program. We find that pro-apoptotic regulators of germline
87 PCD, notably the caspases CED-3 and CSP-1, the BH3-only domain protein CED-13, and regulators
88 of cell corpse engulfment, reduce abundance of a mtDNA deletion and that abrogation of their
89 functions results in elevated levels of the defective mtDNA. Notably, however, loss of the CED-3
90 activator CED-4/Apaf1 [44,45], does not result in elevated levels of defective mtDNA. These
91 findings raise the possibilities that the caspases and the other pro-apoptotic factors function in
92 mtDNA purifying selection by a non-canonical CED-4-independent cell death program or that
93 these pro-apoptotic regulators function in mtDNA purifying selection through a PCD-
94 independent mechanism. We also report that defective mtDNA accumulates in the germline of
95 animals with age and that, although the abundance of the defective mtDNA is reduced in
96 offspring, progeny of older mothers inherit higher levels of the mutant mtDNA than those from
97 young mothers. Intergenerational removal of the defective mtDNA appears to be enhanced in
98 older animals with defective mtDNA quality control. Further, we found that lifespan-extending
99 mutations in both the IIS pathway and the non-IIS-dependent lifespan-regulator CLK-1/MCLK1
100 decrease accumulation of defective mtDNA, and that short-lived mutants show elevated
101 accumulation, implicating molecular regulators of the aging process in mtDNA purifying
102 selection. Our findings reveal that the PCD machinery and the aging program contribute to the
103 removal of mtDNA mutations during germline development and their intergenerational
104 transmission.

105

106 **Results**

107 **The stably maintained mtDNA deletion mutant *uaDf5* contains multiple linked mutations**

108 **resulting in aberrant proteins and shows deleterious effects on growth**

109 To test the role of potential regulatory factors in mtDNA purifying selection, we took

110 advantage of *uaDf5*, a 3.1 kb mtDNA deletion mutation that removes part or all of four protein-

111 coding genes and seven tRNAs (Fig. 1A) [46]. Given the presumably deleterious nature of this

112 defective mtDNA, it was of interest to understand how it is stably transmitted despite active

113 purifying selection processes. While its maintenance at high levels is attributable in part to

114 stabilization by the mitochondrial UPR [25], *uaDf5* persists, albeit at lower levels, in animals

115 lacking this activity. One possible explanation for this phenomenon is that the mutant mtDNA

116 might be maintained in heteroplasmy with an otherwise intact mtDNA carrying a complementing

117 mutation. We sought to test this possibility through deep sequencing of mtDNA isolated from

118 the *uaDf5*-bearing strain. Comprehensive sequence analysis revealed that, in addition to the

119 large deletion, the strain indeed carries a second mtDNA mutation, *w47* (Fig. 1A, Suppl. Fig. 1A,

120 B, C). *w47* is a single base pair deletion in the *nduo-4* gene that causes a frameshift, predicted to

121 result in a truncated NADH dehydrogenase 4 (ND4) protein lacking 321 residues (Suppl. Fig. 1D).

122 ND4 is an essential transmembrane subunit within complex I of the mitochondrial respiratory

123 chain (MRC), which drives NADH-oxidation-dependent transport of protons across the inner

124 mitochondrial membrane [47–49]. While this raised the possibility of two complementing mtDNA

125 genomes, we found that the *w47* mutation is present at the same abundance as the *uaDf5*

126 deletion mutation (~75% of total mtDNA, Suppl. Fig. 1B), strongly suggesting that it resides on

127 the same mtDNA genome. As this second mutation cannot explain stabilization of the defective

128 mtDNA by *trans*-complementation of two deleterious mutations, other mechanisms appear to
129 promote the stable inheritance of *uaDf5*.

130 In addition to the aberrant protein encoded by the *w47* frameshift mutation in *nduo-4*, a
131 second abnormal protein is encoded by the *uaDf5* genome: one end of the deletion results in a
132 fusion protein comprised of the first 185 amino acids of NADH dehydrogenase 1 (ND1, a homolog
133 of the core MT-ND1 transmembrane subunit of complex I of the MRC [47,49,50]), and the last 81
134 amino acids of mitochondrial-encoded cytochrome b (CTB-1/CYTB, a transmembrane subunit of
135 complex III of the MRC [47,49,51]) (Suppl. Fig. 1E). It is conceivable that accumulation of these
136 two abnormal proteins -- the truncated ND4 and the ND1-CYTB fusion protein resulting from *w47*
137 and *uaDf5*, respectively – activate the UPR^{MT}, which has been shown to result in clearance of
138 *uaDf5*, dependent on the ATFS-1 transcription factor [25,27].

139 Animals harboring $mtDNA^{uaDf5}$ are viable and fertile, presumably because they contain
140 intact wildtype mtDNA [46]. However, we found that *uaDf5*-bearing animals displayed a
141 significant reduction in brood size (WT 304 ± 4.8; *uaDf5* 201 ± 8.6 embryos laid, $p < 0.001$) (Fig.
142 1B) and a significant increase in embryonic lethality (WT 1.4 ± 0.2%; *uaDf5* 4.2 ± 0.7%, $p < 0.001$)
143 (Fig. 1C). Additionally, *uaDf5* animals are slow-growing, evident in both the number of hours to
144 reach gravidity (WT 63 ± 0.8; *uaDf5* 76 ± 1.4 hours at 20°C, $p < 0.001$) (Fig. 1D) and the stage of
145 development reached after 60 hours of feeding (WT: adult; *uaDf5:* mid-L4) (Fig. 1E). In contrast,
146 however, we were surprised to find that lifespan was not substantially affected (WT 14 ± 0.4;
147 *uaDf5* 15 ± 0.5 days) (Fig. 1F, Suppl. Fig. 2). Given the significant decline in the majority of fitness
148 parameters tested, we conclude that *uaDf5* is a useful tool for studying mitochondrial disease
149 and mechanisms underlying mtDNA quality control.

150 **PCD regulators promote removal of mtDNA^{uaDf5}**

151 During germline development in *C. elegans*, as many as 95% of nuclei destined to become
152 potential oocytes are eliminated by PCD [39–41,52]. While this process has been proposed to be
153 stochastically determined [39,52], it has also been suggested that it functions to selectively
154 remove all but the most "fit" germline cells. As such, PCD could perform a role in purifying
155 selection in the germline, wherein potential oocytes that undergo PCD are associated with higher
156 levels of defective mtDNA. To test this hypothesis, we introduced *uaDf5* into various PCD mutants
157 and quantified abundance of the defective mtDNA by digital-droplet PCR (ddPCR; see
158 Supplementary Table 1 for list of mutants tested). In a wildtype genetic background, we found
159 that the steady-state fractional abundance of *uaDf5* in populations of 200 day 1 adults (first day
160 of adulthood) is highly reproducible across four separate trials, demonstrating the reliability and
161 robustness of the assay. Our analyses confirmed that mtDNA^{uaDf5} constitutes the major molar
162 fraction of mtDNA in the *uaDf5*-bearing strain by a nearly 3:1 ratio (Suppl. Fig. 3).

163 CED-3 in *C. elegans* is the major executioner caspase in the canonical PCD pathway
164 [38,52,53] and is required for virtually all PCD both in the germline and the soma (Suppl. Fig. 5).
165 We found that two *ced-3* mutations that strongly block PCD [54] showed a significant increase in
166 the ratio of defective to normal mtDNA from a molar ratio of 2.9:1 for *ced-3(+)* to 3.5:1 for *ced-*
167 *3(n717)* and 4.6:1 for *ced-3(n1286)* (Fig. 2A). This effect appears to be exclusively attributable to
168 an increase in mtDNA^{uaDf5} in the PCD-deficient strains, as the abundance of mtDNA^{WT} is not
169 significantly different between the strains. These *ced-3(-)* mutations both localize to the p15
170 domain of the protease portion of CED-3 (Suppl. Fig. 4), consistent with abolition of caspase
171 activity. These findings implicate the CED-3 caspase and its p15 domain in mtDNA quality control.

172 We found that one other mutation located in the p15 domain showed only a very slight increase
173 that was not statistically significant (*n2454:* 2.9:1, Fig. 2B). While it is unclear why this allele
174 showed a weaker effect it is noteworthy that, unlike the other two mutations, which result in a
175 dramatic alteration of the protein, this mutation is predicted to result in a relatively modest (ala
176 → thr) single amino acid substitution.

177 A second caspase in *C. elegans*, CSP-1, also functions, albeit less prominently, in PCD.
178 While loss of CSP-1 alone does not result in a strong reduction in PCD, it synergizes with loss of
179 CED-3 both in PCD and in other caspase-dependent processes (Suppl. Fig. 5) [55–57]. We found
180 that removing CSP-1 in the *csp-1(tm917)* knockout mutant results in a significant increase in
181 mtDNA^{uaDf5} abundance to a molar ratio of 3.9:1 (Fig. 2A). Further, we found that this mutation
182 enhances the effect of the *ced-3(n717)* mutation, increasing the mtDNA^{uaDf5}:mtDNA^{WT} molar
183 ratio from 3.5:1 to 4.7:1 (Fig. 2A). Together these findings demonstrate that caspase activity, and
184 possible PCD-mediated clearance, are crucial for mtDNA quality control and function in purifying
185 selection of defective mtDNA.

186 We sought to further investigate a potential role for PCD in mtDNA purifying selection by
187 evaluating the requirement for the pro-apoptotic factor CED-13, a BH3-only domain protein that
188 acts specifically in the germline to activate PCD [38,58,59]. Consistent with a requirement for PCD
189 in purifying selection, we found that two *ced-13* alleles result in a very substantial increase in the
190 mtDNA^{uaDf5}:mtDNA^{WT} molar ratio (*sv32*: 4.2:1 and *tm536*: 5.1:1) (Fig. 2A), supporting the notion
191 that CED-13 promotes removal of defective mtDNA in the germline. CED-13 functions in PCD by
192 antagonizing the function of mitochondrially localized CED-9/Bcl-2 [58,59], which normally
193 sequesters the apoptosome factor CED-4/APAF1 at mitochondria, preventing it from triggering

194 autocatalytic conversion of the executioner caspase zymogen proCED-3 to its pro-apoptotic
195 protease structure (Suppl. Fig. 5) [60]. An equivalent action is carried out in the soma by the BH3-
196 only protein EGL-1 [60]. *n1950*, a gain-of-function allele of *ced-9* that blocks the interaction of
197 EGL-1 with CED-9 at the mitochondria, results in elimination of PCD in the soma but not the
198 germline [39,52,60,61]. Consistent with the lack of effect of *ced-9(n1950gf)* on germline PCD, we
199 found that the mtDNA^{uaDf5}:mtDNA^{WT} molar ratio was not increased in *ced-9(n1950gf)* mutants
200 (2.2:1) (Fig. 2B). Thus, CED-3, CSP-1, and CED-13 are required both for germline PCD and for
201 removal of mtDNA^{uaDf5}.

202 Cells that undergo PCD are cleared by the surrounding cells in the process of engulfment
203 and degradation, which is implemented through a set of redundant pathways that converge on
204 the CED-10 GTPase [62–65] (Suppl. Fig. 5). Although this engulfment process is necessary
205 primarily for removal of the resultant corpses, it also appears to play an active role in cell killing:
206 inhibition of the engulfment pathway diminishes occurrence of PCD, likely through a complex
207 feedback mechanism [66,67]. Further supporting a role for PCD in purifying selection, we found
208 that single or double mutations of several genes that promote engulfment of cell corpses result
209 in elevated mtDNA^{uaDf5}:mtDNA^{WT} molar ratios, ranging from 3.5:1 to 5.2:1 (4.1:1 for the *ced-*
210 *1(e1735)*, 4.5:1 for *ced-2(e1752)*, 5.2:1 for the *ced-1(e1735); ced-2(e1752)* double mutant, 3.6:1
211 for *ced-10(n1993)*, and 4.8:1 for *ced-10(n3246)*; Fig. 2A).

212 We tested whether generally increased germline PCD alters mtDNA^{uaDf5} abundance by
213 examining the effect of removing the caspase-related factor, CSP-2, which has been shown to
214 play an anti-apoptotic role through inhibition of CED-3 autoactivation in the germline (Suppl. Fig.
215 5) [68]. We found that a loss-of-function mutation in *csp-2*, which elevates germline PCD, did not

216 alter the mtDNA^{uaDf5}:mtDNA^{WT} molar ratio (2.9:1 for the *csp-2(tm3077)* knockout mutation) (Fig.
217 2B). This observation does not conflict with a requirement for PCD in purifying selection: a
218 general increase in PCD in the germline of *csp-2(-)* animals would not be expected *per se* to alter
219 the mechanism that *discriminates* defective from normal mtDNAs and therefore the relative
220 abundance of the two forms.
221
222 **Evidence for non-canonical action of PCD regulators in mtDNA purifying selection**
223 The foregoing results implicate a role for the pro-apoptotic CED-3 and CSP-1 caspases,
224 CED-13, and the CED-1, 2, and -10 cell corpse engulfment factors in mtDNA purifying selection.
225 However, several observations suggest that elimination of normal, physiological germline PCD
226 *per se* is insufficient to increase accumulation of defective mtDNA, or that these factors promote
227 purifying selection through a PCD-independent pathway. Specifically, we observed that the
228 occurrence of PCD does not perfectly correlate with their effects on accumulation of mtDNA^{uaDf5}
229 in particular mutants.
230 First, we found that the *ced-3*(*n718)* allele lowers, rather than elevates, the abundance of
231 mtDNA^{uaDf5} (mtDNA^{uaDf5}:mtDNA^{WT} molar ratio of 1.8:1, Fig. 2C). This effect is likely to be
232 attributable to the nature of the *n718* mutation. The *ced-3* mutations that result in elevated
233 mtDNA^{uaDf5} levels (Fig. 2A) both alter the p15 domain, which is essential to the active caspase
234 function. In contrast, the *n718* mutation changes a residue in the caspase activation and
235 recruitment domain (CARD), located within the prodomain of the CED-3 zymogen, which is
236 removed upon caspase activation, and affects its activation by CED-4 (Suppl. Fig. 4) [44,54]. While

237 *ced-3*(*n718)* strongly compromises PCD, this mutation might not alter CED-3 caspase function in
238 a way that interferes with its role in mtDNA purifying selection.

239 Our surprising finding that while CED-3 activity is required for mtDNA purifying selection,
240 a CED-3 mutation that compromises its activation by CED-4 did not elevate mtDNA^{uaDf5} levels
241 prompted us to investigate the requirement of CED-4 in mitochondrial purifying selection.
242 Consistent with the effect of the *ced-3*(*n718)* mutation, we found that eliminating the function
243 of the pro-apoptotic regulator CED-4, the *C. elegans* orthologue of mammalian APAF1 and
244 upstream activator of CED-3 in the canonical PCD pathway [60,69], did not result in a marked
245 increase in the relative abundance of mtDNA^{uaDf5}: while the mtDNA^{uaDf5}:mtDNA^{WT} molar ratio
246 increased to 3.1:1 in the *ced-4(n1894)* mutant, the effect was not statistically significant.
247 Moreover, the canonical allele *ced-4(n1162)* allele similarly showed no elevation in mtDNA^{uaDf5}
248 (molar ratio = 2.6:1; Fig. 2B). These results suggest that CED-3 caspase functions in mitochondrial
249 purifying selection independent of the caspase-activating factor CED-4.

250

251 **Evidence that decreased fitness, but not lifespan, is attributable to mtDNA^{uaDf5}-induced PCD**

252 Taken together, our results implicate many PCD regulatory factors, and potentially PCD, in
253 the selective clearance of defective germline mtDNAs. Our additional observations suggest that
254 defective mtDNAs may, in fact, *trigger* elevated germline PCD, resulting in the production of
255 fewer mature gametes and progeny. Specifically, we found that the significant decrease in brood
256 size that we observed in *uaDf5*-bearing animals with a wildtype nuclear background is partially
257 suppressed by both *ced-3(-)* and *ced-13(-)* mutations, which prevent PCD (Fig. 2D, Suppl. Fig. 6A),
258 suggesting that elimination of PCD might rescue cells that would otherwise be provoked to die

259 as a result of accumulation of defective mtDNA. Our findings further underscore the observation
260 that accumulation of defective mtDNA in those animals that do survive does not affect longevity,
261 as we found that lifespan is unaltered in these PCD mutants even when the levels of mtDNA^{uaDf5}
262 are nearly doubled (Suppl. Fig. 6B, C).
263

264 **Age-dependent accumulation of mtDNA^{uaDf5} in the germline**

265 Our findings that PCD regulators are required to reduce mtDNA^{uaDf5} abundance, the
266 central role that mitochondria play in PCD [31–33,70], the observed decline of mitochondrial
267 health during the aging process [7,35–37,71–75], and the relationship between excessive PCD
268 and the aging phenotype [34] led us to examine the dynamics of mtDNA^{uaDf5} accumulation as
269 worms age. We measured the fractional abundance of *uaDf5* in adults at progressively increased
270 ages spanning day 1, defined as the first day of egg-laying, through day 10. Day 1 through day 4
271 of adulthood encompasses the time during which nearly all self-progeny are produced. After day
272 4, hermaphrodite sperm become depleted and the animals transition into a post-gravid,
273 progressively aging state [76–78]. By day 10, animals exhibit indications of advanced age. Analysis
274 of the abundance of mtDNA^{uaDf5} revealed a progressive increase throughout gravidity and post-
275 reproductive aging, with the mtDNA^{uaDf5}:mtDNA^{WT} molar ratio increasing from 2.9:1 to 5.5:1 (Fig.
276 3A, Suppl. Fig. 7A). This age-related accumulation of *uaDf5* in adult worms is reminiscent of the
277 accumulation of mtDNA mutations seen in aging mammals [35,73,79] and suggests that *uaDf5* in
278 *C. elegans* may be a useful tool for studying the role that mtDNA mutations play in aging.

279 It is conceivable that the age-dependent increase in mtDNA^{uaDf5} is attributable to
280 accumulation in somatic mitochondria, as gametes are depleted with age. To assess whether the

281 observed age-related accumulation of mtDNA^{uaDf5} occurs predominantly in the maternal
282 germline or in somatic cells, we analyzed animals defective in germline development by taking
283 advantage of the *glp-4(bn2)* mutant, which produces only a small number (~12) of germline cells
284 compared to that in wildtype animals (~1,500), with no known effect on somatic gonad
285 development [80]. In contrast to the increased mtDNA^{uaDf5} abundance with age seen at
286 permissive temperature (mtDNA^{uaDf5}:mtDNA^{WT} of 1.8:1 at day 1, rising to 2.6:1 at day 4, for an
287 overall increase by 48%), we found that *glp-4(bn2)* animals at the non-permissive temperature
288 showed a slight decrease in the defective mtDNA from day 1 to day 4 of adulthood (2.2:1 at day
289 1, dropping to 2:1 at day 4, for an overall decrease of 6.3%) (Fig. 3B). These results strongly
290 suggest that the observed age-dependent increase in mtDNA^{uaDf5} abundance occurs exclusively
291 in the germline. We found that mtDNA^{uaDf5} does eventually appear to accumulate in somatic cells
292 with age, as day 10 adults grown at the restrictive temperature showed a marked increase in the
293 mtDNA^{uaDf5}:mtDNA^{WT} molar ratio compared to day 1 adults even in the absence of a germline
294 (day 10 *glp-4(bn2)* molar ratio of 3.4:1, a 57% increase from day 1 levels) (Fig. 3B). Similar effects
295 were observed in animals lacking a maternal germline as a result of a masculinizing gain-of-
296 function mutation in the *fem-3* gene (Fig. 3B) [81]. We conclude that the marked increase in
297 mtDNA^{uaDf5} with age during the period of fecundity occurs primarily in the germline and that the
298 defective mtDNA accumulates in both germline and somatic tissue during post-reproductive life.
299

300 **Age-dependent increase in mtDNA^{uaDf5} burden is transmitted to progeny**

301 As the mtDNA is inherited strictly through the maternal germline, we posited that the
302 age-dependent increase in the fractional abundance of germline mtDNA^{uaDf5} might be

303 transmitted to progeny animals. To test this hypothesis, we measured the molar ratio of
304 mtDNA^{uaDf5} in 200-worm populations of L1 larvae derived from day 1 – day 4 adults (Fig. 3C,
305 Suppl. Fig. 7B). This analysis led to two key observations: 1) the abundance of mtDNA^{uaDf5} is
306 reduced during transmission between mother and offspring (average decrease ranging from 6%
307 to 13%), presumably as a result of purifying selection, and 2) the abundance of the defective
308 mtDNA in the offspring correlates with the age of the mothers: progeny of older mothers contain
309 a substantially higher mtDNA^{uaDf5}:mtDNA^{WT} molar ratio (4.2:1) than that of younger mothers
310 (2.6:1) (Fig. 3C, D). A similar trend was observed for mother-to-offspring transmission in five
311 mutant strains with altered levels of mtDNA^{uaDf5} (see below): in all cases, progeny contain lower
312 abundance of mtDNA^{uaDf5} than their mothers, and progeny of younger adults inherit a lower load
313 of mtDNA^{uaDf5} than progeny of older adults (Fig. 3C). These results reveal that mtDNA quality
314 control occurs between primordial germ cell proliferation in the female germline and L1 hatching,
315 i.e., during oocyte maturation, embryogenesis, or both.
316
317 **The lifespan-determining IIS pathway regulates accumulation of mtDNA^{uaDf5}**
318 We sought to determine whether the age-dependent accumulation of defective mtDNA
319 is controlled by known molecular mechanisms that drive the aging program in *C. elegans*. The
320 most prominent of these regulatory systems is the highly conserved insulin/IGF-1 (insulin-like
321 growth factor-1) pathway (IIS), which performs a pivotal regulatory function in aging and
322 longevity [28,82,83] (Suppl. Fig. 8). Abrogation of the IIS signaling pathways, for example, as a
323 result of mutations in the gene encoding the IIS receptor (DAF-2, in *C. elegans*), results in
324 substantial slowing of the aging program and extension of lifespan in worms, flies, and mice [84–

325 87]. The IIS pathway also functions in a broad set of other processes including, in *C. elegans*,
326 activation of two stages of developmental arrest, or diapause, at the L1 larval stage and in
327 formation of the dispersal form, the dauer larva, as well as in the control of germline
328 proliferation, stress resistance, fat metabolism, and neuronal/behavioral programs [28]. It was
329 recently reported that inhibition of the IIS pathway rescues various fitness parameters in a
330 mtDNA mutator strain which contains a faulty mtDNA polymerase [29], consistent with a possible
331 role in mtDNA quality control.

332 We found that two mutant alleles of *daf-2*, which reduce rates of aging and increase
333 lifespan, result in dramatically decreased mtDNA^{uaDf5}:mtDNA^{WT} molar ratios from 2.8:1 to as low
334 as 0.3:1 (0.3:1 for *daf-2(e1391*); 0.8:1 for *daf-2(e1370)*; Fig. 4A; see Suppl. Table 2 for a list of
335 lifespan mutants used in the analyses). Thus, the lifespan-extending effects of *daf-2* mutations
336 are strongly correlated with diminished abundance of defective mtDNA, to the extent that it
337 becomes the minor species of mtDNA.

338 The DAF-2 receptor acts by antagonizing the DAF-16/FoxO transcription factor, the major
339 effector of IIS downstream, in response to insulin-like ligands. Thus, removal of *daf-16* function
340 reverses the lifespan-extending effects of *daf-2(-)* mutants. We tested whether the DAF-2 → DAF-
341 16 pathway similarly functions in mtDNA purifying selection. We found that eliminating DAF-16
342 in two *daf-16* mutants results in slightly increased, albeit not statistically significant,
343 mtDNA^{uaDf5}:mtDNA^{WT} molar ratios (3.3:1 for *daf-16(mu86)*; 3.5:1 for *daf-16(mgDf50)*) (Fig. 4B).
344 Further, we found that, in double mutants, removal of DAF-16 in the *daf-16(mu86)* mutation
345 suppressed the decreased mtDNA^{uaDf5}:mtDNA^{WT} molar ratios observed in two *daf-2* mutants,
346 from 0.3:1 for *daf-2(e1391)* to 1:1 for *daf-16(mu86); daf-2(e1391)* and from 0.6:1 for *daf-*

347 *2(e1370)* to 1.8:1 for *daf-16(mu86); daf-2(e1370)*, consistent with observations reported in a
348 recent study [88]. While the *daf-2(-)* effect on mtDNA^{uaDf5} levels is largely dependent on DAF-16,
349 neither double mutant returned mtDNA^{uaDf5} levels to those seen in animals with a fully intact IIS
350 pathway, suggesting that other DAF-2 targets might participate in removal of defective mtDNA
351 (Fig. 4C). We found, conversely, that two mutations that reduce lifespan by eliminating the
352 function of AAK-2 (AMP activated kinase-2), a conserved factor acting in the IIS pathway [28,89],
353 result in elevated mtDNA^{uaDf5}:mtDNA^{WT} molar ratios as high as 4.4:1 compared to 2.8:1 in
354 wildtype animals (3.8:1 for *aak-2(ok524)* and 4.4:1 for *aak-2(gt33)*) (Fig. 4B). These findings
355 demonstrate that alterations in the IIS pathway coordinately affect both lifespan and
356 accumulation of defective mtDNA and that the DAF-2/DAF-16/AAK-2 axis acts similarly in both
357 processes.
358
359 **Synergistic effect of multiple aging pathways on mtDNA^{uaDf5} accumulation**
360 In addition to IIS, other molecular regulatory pathways independently contribute to the
361 rate of aging. These include CLK-1, a mitochondrial hydroxylase that functions in the pathway for
362 ubiquinone synthesis [90,91]. *clk-1* mutants with a wildtype mitochondrial genome have been
363 shown to contain levels of mtDNA that are elevated by 30%, perhaps as the result of a
364 compensatory process that increases demand on mitochondrial abundance or the action of CLK-
365 1 as a regulator of mtDNA abundance in response to energy availability within the cell [92]. As
366 with long-lived *daf-2* mutants, we found that long-lived *clk-1(qm30)* mutants showed a greatly
367 decreased mtDNA^{uaDf5}:mtDNA^{WT} molar ratio of 0.3:1 (Fig. 4A), comparable to that in *daf-2*
368 mutants; again, mtDNA^{uaDf5} is the minor species in these animals. As the IIS and CLK-1 appear to

369 act separately in controlling lifespan, we postulated that elimination of both mechanisms might
370 further reduce levels of the defective mtDNA. Indeed, we found that mtDNA^{uaDf5} was completely
371 eliminated in *daf-2(e1391) clk-1(qm30)* double mutants, revealing a strongly synergistic effect
372 between the two age-determining systems (Fig. 4A). Thus, distinct regulatory pathways for
373 longevity modulate the abundance of mtDNA^{uaDf5} by apparently different mechanisms and
374 elimination of the two pathways abrogates its maintenance, providing insights into processes
375 that might prevent accumulation of defective mtDNAs.
376
377 **Age-dependent accumulation rate of mtDNA^{uaDf5} strongly correlates with genetically altered**
378 **rates of aging**
379 Our findings that the steady-state abundance of mtDNA^{uaDf5} increases with maternal age
380 and that mutants with increased lifespan show lower levels of the defective mtDNA raised the
381 possibility that purifying selection is under the same control as aging clocks. To assess this
382 potential connection, we analyzed the time-dependent rates of mtDNA^{uaDf5} accumulation in
383 animals with genetic backgrounds that alter the aging clock. Analysis of 24 different genetic
384 backgrounds over the first ten days of adulthood revealed that the age-dependent progressive
385 accumulation of mtDNA^{uaDf5} is a consistent phenomenon (Fig. 4D). Comparison of long-lived
386 mutants and wildtype using a linear regression model revealed a striking positive correlation
387 between aging rate and age-dependent rate of accumulation of mtDNA^{uaDf5}: all long-lived
388 mutants in either the IIS pathway or *clk-1* accumulate mtDNA^{uaDf5} at a substantially slower rate
389 as they age than do wildtype animals (Fig. 4E, Suppl. Fig. 9A, B). Conversely, we analyzed six short-
390 lived IIS pathway mutant combinations and found that the *aak-2(ok524)* and *daf-16(mu86)* single

391 mutants and *daf-16(-);daf-2(-)* double mutants all showed increased rates of mtDNA^{uaDf5}
392 accumulation (Fig. 4E, Suppl. Fig. 9C, D). These observations suggest that in both slower-aging
393 and faster-aging strains, the rate of accumulation of deleterious mtDNA is a predictor of aging
394 rate. In the two exceptional cases, the *aak-2(gt33)* and *daf-16(mgDf50)* single mutants, we did
395 not observe an increased accumulation rate compared to wildtype; however, the mtDNA^{uaDf5}
396 levels are consistently higher than in these two mutants than in wildtype at all stages (Fig. 4E,
397 Suppl. Fig. 9D) and thus, diminished removal of mtDNA^{uaDf5} overall correlates with decreased
398 lifespan in these mutants as well. The greater mtDNA^{uaDf5} accumulation rates seen in the short-
399 lived animals is not attributable to the higher steady-state levels *per se*, as the rates of
400 accumulation of defective mtDNA observed in the PCD mutants with higher mtDNA^{uaDf5} levels
401 show no correlation with the steady-state levels (Suppl. Fig. 9 E-H); rather these increased rates
402 appear specifically to be a property of the shortened lifespan mutants.

403 Consistent with a relationship between aging rates and accumulation of defective mtDNA,
404 we found that brood size is decreased and embryonic lethality is increased in short-lived *daf-16*
405 mutants compared to those in a wildtype nuclear background, while *uaDf5* does not impact
406 either fitness parameter in the long-lived *clk-1* mutant (Suppl. Fig. 10). These results are
407 consistent with the possibility that longevity pathways modulate fitness in part by regulating
408 mitochondrial homeostasis.

409

410 **Evidence for late adulthood-specific mechanisms for removal of mtDNA^{uaDf5}**

411 We obtained evidence that defective mtDNA is more effectively removed in offspring of
412 aging adults that carry an unusually high burden of mtDNA^{uaDf5}. The offspring of day 4 adults in

413 those strains ("high" strains) with significantly higher steady-state fractional abundance of
414 mtDNA^{uaDf5} showed significantly greater rates of reduction of the defective mtDNA (reduction
415 from 5.4:1 to 3.3:1 in *atfs-1(et15)*, from 6.5:1 to 2.8:1 in *ced-10(n1993),* and from 6.4:1 to 3.3:1
416 in *ced-13(sv32)*) compared to offspring of ("low" strain) mothers with lower steady-state
417 fractional abundance of the mutant mtDNA (reduction from 4.7:1 to 4.2:1 in WT, from 3.9:1 to
418 2.8:1 in *ced-3(n2454),* and from 3.2:1 to 2.5:1 in *ced-4(n1162)*). Thus, day 4 progeny from "high"
419 strains actually inherit a lower mtDNA^{uaDf5} load than their siblings born from day 1-3 mothers (Fig.
420 3C, 5A). Indeed, we found a strong correlation (r^2=0.61, $p < 0.001$) between the steady-state level
421 of mtDNA^{uaDf5} in mothers and the capacity for its removal between mother and progeny during
422 day 4 of adulthood (Fig. 5B). These results raise the possibility that very high levels of mtDNA^{uaDf5}
423 in older mothers may activate additional mtDNA purifying selection (independent of the UPR^{MT}
424 and PCD machinery), thereby ensuring that progeny are not overloaded with defective
425 mitochondria.
426

427 **Discussion**

428 We have obtained several lines of evidence indicating that regulators of PCD and the aging
429 program function in mtDNA quality control and accumulation of defective mtDNA in *C. elegans*.
430 We report eight major findings: 1) regulators of germline PCD are required for effective removal
431 of deleterious mtDNA from the germline; 2) the cell death machinery functions in either a non-
432 canonical cell death pathway or in a non-apoptotic role to mediate mitochondrial purifying
433 selection; 3) the CSP-1 caspase has a larger effect on mitochondrial purifying selection than the
434 major PCD regulator CED-3; 4) mtDNA^{uaDf5} progressively accumulates in the germline as adults
435 age; 5) this age-dependent accumulation of mtDNA^{uaDf5} is transmitted to progeny; however, the
436 burden of the defective mtDNA is lower in offspring than mothers, suggesting intergenerational
437 purifying selection; 6) two separate aging pathways, the IIS and CLK-1 pathways, act
438 synergistically to regulate mtDNA^{uaDf5} levels; longer-lived mutants show reduced levels of the
439 defective mtDNA while shorter-lived mutants show increased levels compared to otherwise
440 wildtype animals; 7) the rate of mtDNA^{uaDf5} accumulation is inversely correlated with lifespan in
441 aging mutants; 8) intergenerational removal of mtDNA^{uaDf5} occurs more effectively during
442 transmission from older mothers with high burden of the defective mtDNA.

443 Previous reports demonstrated that UPR^{MT} limits *uaDf5* clearance, and that eliminating
444 the UPR^{MT}-mediating transcription factor, ATFS-1, lowers mtDNA^{uaDf5} abundance [25,27]. Our
445 identification of a second mutation in the *uaDf5* mutant that results in premature truncation of
446 the ND4 gene product raises the possibility that expression of both the truncated ND4 and the
447 ND1-CYTB fusion protein might together activate UPR^{MT}. The possibility that it is the production

448 of aberrant polypeptides resulting from these mutations that trigger this response will require
449 analysis of additional mtDNA mutants.
450
451 **Mitochondrial deletion mutant *uaDf5* as a model for mitochondrial disease**
452 We found that *uaDf5* affects brood size, embryonic lethality, and developmental rate,
453 highlighting its use as a model for investigating mitochondrial diseases. The reduced brood size
454 in *uaDf5*-bearing animals might reflect diminished germ cell proliferation, as mitochondria have
455 been implicated in progression of germline maturation [93,94]. Alternatively, the defective
456 mtDNA might trigger hyperactivation of germline PCD pathway that specifically removes germ
457 cells with the highest burden of defective mtDNA, as suggested by our results, resulting in the
458 survival of fewer mature oocytes. The increased embryonic lethality in the *uaDf5* strain may be
459 a consequence of a genetic bottleneck effect, leading to rapid differences in mtDNA allele
460 frequencies [95–97] and a subpopulation of oocytes containing levels of mtDNA^{uaDf5} that exceed
461 a threshold required for viability.
462 We were surprised to find, in contrast to a previous report [98], that mtDNA^{uaDf5} did not
463 alter lifespan. Given that mitochondrial mutations are often coupled with compensatory
464 mutations in the nuclear genome [99–103], one possible explanation for this discrepancy might
465 be that a compensatory nuclear mutation exists in the strain analyzed, diminishing the impact of
466 the defective mitochondrial genome. We note, however, that we backcrossed the *uaDf5* strain
467 extensively to the laboratory reference strain N2 prior to performing the reported analyses. It is
468 conceivable that although we observed no effect in the lab, *uaDf5* might alter lifespan under
469 natural conditions. Exposure to increased stress from growth in the wild might be less tolerated

470 in animals bearing mtDNA^{uaDf5}, as has been observed with other mitochondrial mutants [104],
471 resulting in diminished lifespan.
472
473 **Caspases and cell death machinery regulate mitochondrial purifying selection**
474 Our results lend support to the hypothesis that germline PCD mechanisms may be used
475 to cull germline cells with defective mtDNA (Fig. 6A). Developmentally programmed cell death
476 and cell death in response to genotoxic stress are mediated by caspases upon activation by the
477 *C. elegans* octameric apoptosome which is formed when the inhibition of CED-4 by CED-9 is
478 disrupted through the binding of BH-3-only proteins EGL-1 and CED-13 in the soma and germline,
479 respectively. We propose that in response to mitochondrial genotoxic stress (increased
480 mtDNA^{uaDf5} load), caspases CED-3 and CSP-1 that are activated by the BH-3 only domain protein
481 CED-13, trigger mitochondrial purifying selection, independent of CED-9 and the CED-4
482 apoptosome, either through germ cell PCD or reflect a non-apoptotic role of these caspases (Fig.
483 6A).
484 Mutations that eliminate the function of caspases that act in PCD result in elevated
485 mtDNA^{uaDf5} levels. Two of three mutants affecting the p15 domain of the CED-3 caspase result in
486 a significantly increased molar ratio of *uaDf5*, highlighting the importance of the p15 domain in
487 mtDNA quality control. It is noteworthy that the two mutations that result in a more substantial
488 effect on mtDNA^{uaDf5} abundance affect CED-3 structure more dramatically: *ced-3(n717)* results in
489 a splicing error, and *ced-3(n1286)* is a nonsense mutation [54]. In contrast, *ced-3(n2454)*, which
490 results in a subtle (statistically insignificant) increase in mtDNA^{uaDf5} is a substitution predicted to
491 impart a much weaker effect on the protein structure [54]. The effect of the *ced-3(n718)* allele,

492 which resides in the prodomain of CED-3, suggests that that portion of the protein may act to
493 inhibit mtDNA quality control. Taken together, our results suggest that CED-3 may carry out a
494 specialized activity in mtDNA-activated PCD. We found that a second caspase, CSP-1, which plays
495 a minor role in PCD [56,57]) is also required in mtDNA quality control: a *csp-1(-)* knockout
496 mutation results in increased abundance of mtDNA^{uaDf5} and enhances the effect of *ced-3(n717)*,
497 suggesting that CSP-1 may play a larger role in removal of defective mtDNA than it does in other
498 forms of PCD. An exciting possibility is that caspases act in mtDNA quality control via a mechanism
499 that is distinct from their normal action in PCD. Such putative roles for caspases and other
500 mitochondrial factors in non-apoptotic mitochondrial quality control may have been co-opted
501 during metazoan evolution with the innovation of PCD.

502 Analysis of additional PCD components further implicate a role for germline PCD in
503 mitochondrial purifying selection. These include CED-13, the germline-specific PCD effector, and
504 components of the cell corpse engulfment pathway, which activate PCD likely through a complex
505 feedback mechanism that ensures cells destined to die proceed irreversibly through the process
506 [66,67]. In all cases, mutations in these components result in increased mtDNA^{uaDf5} levels. In
507 vertebrates, mitochondrial reactive oxygen species (mtROS) trigger apoptosis via the intrinsic
508 mitochondrial pathway [120]. Interestingly, elevated mtROS promotes longevity that is, in part,
509 dependent on the core cell death machinery in *C. elegans*, involving CED-9, CED-4, CED-3 and
510 CED-13, but not EGL-1 [105]. In that study, the authors reported that the protective effect of the
511 cell death machinery on lifespan was independent of PCD in the soma; however, germline cell
512 death was not characterized. Given that CED-13, and not EGL-1, is the predominant BH3-domain
513 protein functioning in the germline [58] and that ablation of germline leads to extended lifespan

514 [106], our findings support the possibility that germline progenitors carrying defective
515 mitochondria selectively undergo PCD, ensuring homeostatic mtDNA copy number and health of
516 progeny.

517 A striking exception to our findings was seen with mutations that eliminate the function
518 of the pro-apoptotic regulator CED-4. Neither the *ced-3(n718)* mutation that disrupts the CED-3
519 CARD domain, which is involved in recruitment to the apoptosome by stabilizing its interaction
520 with CED-4 [44,107], nor *ced-4(-)*, result in increased accumulation of mtDNA^{uaDf5}, suggesting
521 non-canonical, CED-4-independent activation of CED-3 in mitochondrial purifying selection. It is
522 possible that the CARD mutation (G65R) in *ced-3(n718)* [54] reduces the fraction of CED-3 in
523 complex with the apoptosome, which might release more of the protein for its role mitochondrial
524 purifying selection. Interestingly, the CARD linker domain has been found to have an inhibitory
525 effect on the pro-caspase-9 zymogen [108]. *ced-3(n718)* could be effectively acting as a gain-of-
526 function allele in the process of purifying selection, reflected by the lower levels of mtDNA^{uaDf5} in
527 this mutant background.

528 It is noteworthy that CED-4 and its mammalian Apaf1 relatives regulate a variety of
529 cellular functions that are unrelated to their activities in PCD. These include cell growth control
530 influenced by DNA damage, centrosomal function and morphology, neuronal regeneration, and
531 inhibition of viral replication [109–112]. In addition, as a result of differential RNA splicing, *ced-4*
532 encodes proteins with opposing activities, generating both an activator and a repressor of
533 apoptosis [113], which further complicates analysis of its action. Thus, it is conceivable that CED-
534 4 might exert opposing effects on purifying selection, reflecting its pleiotropic activities in
535 development and confounding an unambiguous interpretation of its action in this process.

536

537 **IIS and CLK-1 synergistically regulate germline accumulation of mtDNA^{uaDf5} as adults age**

538 We found that most of the increase in the fractional abundance of mtDNA^{uaDf5} as worms
539 age throughout the period of self-fertility (days 1-4) occurs in the germline. However, the relative
540 amount of the defective mtDNA continues to increase in older animals, when the germline is no
541 longer actively proliferating [76], suggesting that proliferation also occurs in somatic tissues
542 throughout the aging process. This behavior mirrors the dynamics of mutant mtDNAs observed
543 in other organisms, including human, mouse, rat, and rhesus monkey [35,73,79]. While removal
544 of the germline in worms results in extended lifespan [114,115], it is not clear whether, or to
545 what extent, this increased lifespan might be attributable to accumulation of mutant mtDNA,
546 since the lack of germline leads to a variety of cellular responses [116,117], any of which might
547 lead to lifespan extension.

548 These studies do not reveal whether, or how, aging and accumulation of defective mtDNA
549 are causally linked. However, our findings that steady-state levels of mtDNA^{uaDf5} are lowered in
550 long-lived mutants (*daf-2* (IIS pathway; [28]) and *clk-1* (mitochondrial function; [118,119])) and
551 that rates of its accumulation are strongly inversely correlated with lifespan extension through
552 independent pathways, suggesting that mtDNA purifying selection mechanisms are influenced
553 by aging programs (Fig. 6A). Further bolstering this potential link is our finding that short-lived
554 mutants (*daf-16* and *aak-2,* both involved in the IIS pathway [28]), show higher steady-state levels
555 of mtDNA^{uaDf5}. That this effect is greater in *aak-2* mutants than in *daf-16* mutants suggests that
556 the AAK-2 branch of the IIS pathway influences mtDNA quality control more significantly than
557 does the DAF-16 branch. One of the substrates of AAK-2 is SKN-1/Nrf2, a multifaceted

558 transcription factor with roles in stress response and longevity, and one of its isoforms, SKN-1a,
559 localizes to the mitochondrial surface [120], raising the possibility that AAK-2 might influence
560 clearance of defective mtDNA through SKN-1 action. It will be of interest to assess how defective
561 mtDNA might coordinately trigger quality control and stress-response pathways.

562 Our observation that IIS pathway components and CLK-1 act synergistically on the mtDNA
563 quality control machinery raises the possibility that these two distinct lifespan-regulating
564 pathways converge on a common system for removal of defective mtDNA, such as a global
565 mitochondrial stress response pathway. Candidates for mediating this removal process include
566 mitochondrial fission/fusion [17,20,121], mitophagy [18,19,122], and the UPR^{MT} [22–27], all of
567 which are known to act in mtDNA quality control, as well as modulation of the regulatory
568 pathway for PCD, as suggested by our findings.

569

570 **PCD is uncoupled from aging during intergenerational mitochondrial purifying selection in**
571 **older mothers**

572 Analysis of newly hatched L1 larvae revealed that the relative load of $mtDNA^{uaDf5}$ is
573 transmitted from mother to offspring, with evidence for intergenerational purifying selection
574 (Fig. 6B). This finding implies that mtDNA quality control occurs between germline stem cell
575 expansion in the mature female germline and L1 hatching, a developmental period that spans
576 many potential stages at which it might occur, including germline PCD, oocyte maturation, and
577 the entirety of embryogenesis. It is conceivable that this selection process acts at multiple stages
578 throughout this developmental window and that the decreased burden of defective mtDNA in

579 newly hatched L1 larvae reflect the summation of a series of sequentially acting processes that
580 incrementally enrich for healthy mtDNA.

581 The efficacy of intergenerational removal of mtDNA^{uaDf5} increases in old mothers,
582 including in strains lacking pro-apoptotic regulators. The clearance is particularly precipitous in
583 strains with a very high burden of defective mtDNA as seen in the absence of CED-13, CED-10,
584 and ATFS-1, suggesting a critical threshold beyond which a germline PCD-independent mtDNA
585 quality control process may be initiated or elevated in these older mothers (Fig. 6B). One possible
586 explanation for this observation is that an mtDNA purifying selection mechanism that is typically
587 inhibited by germline PCD might be activated in older mothers. This unidentified purifying
588 selection mechanism might be triggered by the unique cellular environment associated with
589 aging, such as increased organelle or macromolecule damage. Alternatively, the effect might be
590 the result of an age-dependent genetic program.

591 While our study has uncovered new mechanisms acting in mtDNA purifying selection and
592 its relationship to aging, it is of note that some level of mtDNA^{uaDf5} is maintained in all but the
593 most extreme conditions we have observed (e.g., in the *daf-2(e1391) clk-1(qm30)* double mutant,
594 in which the defective mtDNA is extirpated). This finding raises the possibility that some degree
595 of heteroplasmy, even with defective mtDNA, is not only tolerated, but may be adaptive by
596 providing a degree of evolutionary plasticity. Cells might purposefully allow for limited
597 heteroplasmy as a way of increasing genetic heterogeneity that might prove evolutionarily
598 advantageous. Such heterogeneity may also be essential to allow mtDNA to co-evolve with
599 changes arising in the nuclear genome. It may be that a dynamic balance between active mtDNA

600 purifying selection, including the mechanisms identified here, and the permissibility of limited

601 heteroplasmy, is modulated according to environmental or physiological demands.

602

603

604 **Materials and Methods**

605 **Culturing of nematodes**

606 Nematode strains were maintained on NGM plates as previously described at either 20°C
607 or 15°C for the temperature-sensitive strains [123]. Supplementary Tables 1, 2 and 3 provide
608 details of all strains used in this study. Strains without a JR designation were either provided by
609 the CGC which is funded by NIH Office of Research Infrastructure Programs (P40 OD010440) or
610 were obtained from the Mitani lab (strains with a FX designation or JR strains containing alleles
611 with a tm designation were generated from Mitani lab strains) [124].

612 **Population collection by age**

613 Upon retrieval of a stock plate for a given strain, three chunks were taken from the stock
614 plate and placed onto three separate large NGM plates to create three biological replicates
615 ("lines"). Each of these lines was chunked approximately each generation to fresh large NGM
616 plates (every 3 days if maintained at 20°C or 25°C, or every four days if maintained at 15°C, being
617 careful to not let the worms starve between chunks). After four generations of chunks, an egg
618 prep was performed on each line (as described previously; [123]) and left to spin in M9 overnight
619 to synchronize the hatched L1s. The next day, each egg prep was plated onto three large seeded
620 plates at an equal density and the worms were left to grow to day 2 adults (second day of egg
621 laying). The day 2 adult worms were egg prepped for synchronization and left to spin in M9 buffer
622 overnight. The next day, each egg prep was plated onto five large NGM plates at equal density.
623 Once the worms reached day 1 of adulthood (first day of egg-laying), one of the plates was used
624 to collect 200 adult worms by picking into 400 μl of lysis buffer, and the remaining adults on the
625 plate were egg prepped for the collection of hatched L1 larvae in 400 μl lysis buffer the following

626 day. The worms on the four remaining plates were transferred to a 40 μm nylon mesh filter in
627 order to separate the adults from the progeny, and the resulting adults were resuspended in M9
628 and pipetted onto fresh large NGM plates. This process was repeated for the following three days
629 (Day 2-4 of adulthood). Day 5-10 adults were moved to fresh NGM plates every 2nd day using a
630 40 μm nylon mesh filter, and the resulting day 10 adults were collected in lysis buffer.

631 **ddPCR**

632 The worm lysates were incubated at 65°C for 4 hours and then 95°C for 30 minutes to
633 deactivate the proteinase K. Each lysate was diluted; 100-fold for 200 worm adult population
634 lyses, 2-fold for 200 worm L1 population lyses, and 25-fold for individual adult lyses. 2 μl of the
635 diluted lysate was then added to 23 μl of the ddPCR reaction mixture, which contained a
636 primer/probe mixture and the ddPCR probe supermix with no dUTP. The primers used were:

637 WTF: 5'-GAGGGCCAACTATTGTTAC-3'

638 WTR: 5'-TGGAACAATATGAACTGGC-3'

639 UADF5F: 5'-CAACTTTAATTAGCGGTATCG-3'

640 UADF5R: 5'-TTCTACAGTGCATTGACCTA-3'

641 The probes used were:

642 WT: 5'-HEX-TTGCCGTGAGCTATTCTAGTTATTG-Iowa Black® FQ-3'

643 UADF5: 5'-FAM-CCATCCGTGCTAGAAGACAAAG- Iowa Black® FQ-3'

644 The ddPCR reactions were put on the BioRad droplet generator and the resulting droplet-
645 containing ddPCR mixtures were run on a BioRad thermocycler with the following cycle
646 parameters, with a ramp rate of 2°C/sec for each step:

647 1. 95°C for 5 minutes

648 2. 95°C for 30 seconds

649 3. 60°C for 2 minutes

650 4. Repeat steps 2 and 3 40x

651 5. 4°C for 5 minutes

652 6. 90°C for 5 minutes

653 After thermocycling, the ddPCR reaction plate was transferred to the BioRad droplet reader and
654 the Quantasoft software was used to calculate the concentration of mtDNA^{uaDf5} (FAM positive
655 droplets) and mtDNA^{WT} (HEX positive droplets) in each well.

656 **Lifespan analysis**

657 Confluent large plates were egg prepped and left to spin in M9 overnight for
658 synchronization. The hatched L1s were plated onto large thick plates and allowed to grow to day
659 2 adults before being egg prepped a second time and left to spin in M9 overnight. The next
660 morning, referred to as day 1 for lifespan determination, L1s were singled out onto small plates.
661 Once the worms started laying eggs, they were transferred each day to a fresh small plate until
662 egg laying ceased, after which the worms remained on the same plate unless bacterial
663 contamination required transfer to a fresh plate. Worms were considered dead if there was no
664 movement after being lightly prodded with a worm pick. Worms that died due to desiccation on
665 the side of the plate were excluded from analysis.

666 **Brood size and embryonic lethality analysis**

667 Confluent large plates were egg prepped and left to spin in M9 overnight for
668 synchronization. The hatched L1s were plated onto large thick plates and allowed to grow to day
669 2 adults before being egg prepped a second time and left to spin in M9 overnight. The next

670 morning, L1s were singled out onto small plates. Once the worms started laying eggs, they were
671 transferred each day to a fresh small plate until egg laying ceased. The day after transfer to a
672 fresh plate, unhatched embryos and hatched larvae on the plate from the previous day were
673 counted. This was done for each of the days of laying and the total of unhatched embryos and
674 hatched larvae from all plates from a single worm were tabulated to determine total brood size.
675 To determine embryonic lethality, the total number of unhatched embryos was divided by the
676 total brood size. Worms that died due to desiccation on the side of the plate were excluded from
677 analysis.

678 **Developmental time course analysis**

679 Confluent large plates were egg prepped and left to spin in M9 overnight for
680 synchronization. The hatched L1s were plated onto large thick plates and allowed to grow to day
681 2 adults before being egg prepped a second time and left to spin in M9 overnight. The next
682 morning, L1s were singled out onto small plates. The stage of the worms was assayed every 12
683 hours for the first 72 hours after plating. For determining the stage at 60 hours, L4 worms were
684 divided up into three subgroups based on morphology: young-L4, mid-L4, and late-L4; otherwise,
685 all other staged worms were not divided up into subgroups. Worms that died due to desiccation
686 on the side of the plate were excluded from analysis.

687 **Genotyping the *w47* allele**

688 DNA was collected from reference strain (N2) and two *uaDf5*-containing strains, LB138
689 and JR3630. Mitochondrial DNA was extracted and the DNA libraries were prepared using
690 Nextera Kit and then sequenced using an Illumina NextSeq500. Prior to alignment, reads from
691 fastq files were trimmed using Trimmomatic. Trimmed, pair-end reads (2x150) were then

692 mapped to the *C. elegans* assembly reference sequence WBcel235 using Burrows-Wheeler
693 Aligner (BWA) [125]. Picard Tools (http://broadinstitute.github.io/picard/) was used to mark
694 duplicate reads, and SAMtools [126] was used to merge, index and create pile-up format. VarScan
695 [127] was used to call variants, and only variants with minimum coverage of 100 and a minimum
696 variant frequency call of 0.01 were considered for analysis.

697 **Statistical Analysis**

698 Summary statistics, ANOVA, Mann-Whitney tests, and linear regression were calculated
699 using R v3.4.1. The details of the statistical tests are reported in the figure legends.

700

701 **Figures**

702 **Figure 1**

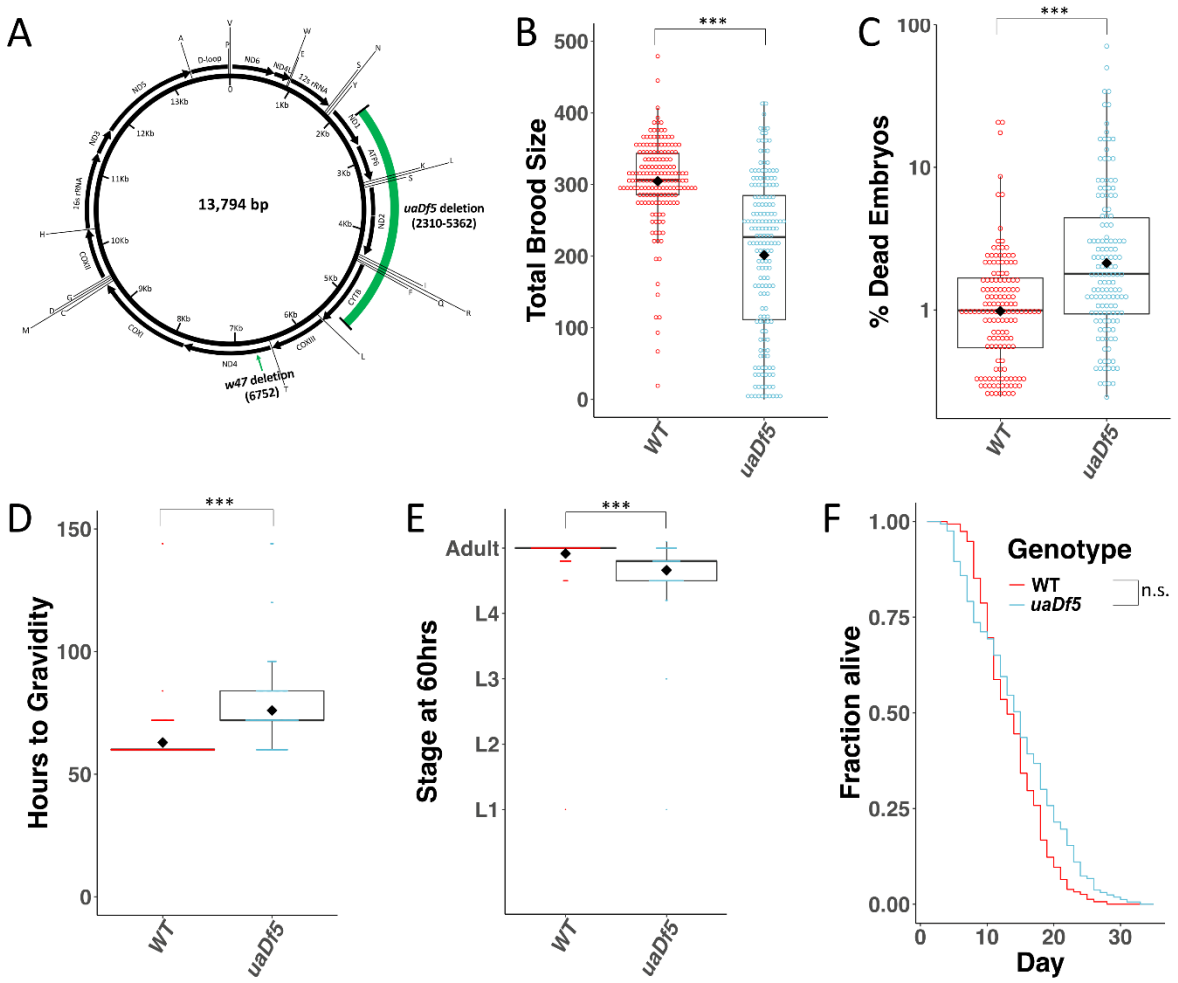

703

704 **Figure 1: Analysis of the impact of mtDNA^{uaDf5} on fitness parameters. (A)** Diagram of *C. elegans*

705 mtDNA. Black bars with arrows indicate the locations of genes and direction of transcription.

706 Black lines with letters indicate the locations of tRNAs. Green bars show the locations of the

707 mtDNA^{uaDf5} deletion as well as the linked *w47* deletion that was identified via Illumina

708 sequencing. **(B)** Brood size analysis of mtDNA^{uaDf5} compared to laboratory wildtype N2. **(C)**

709 Embryonic lethality analysis of *uaDf5* compared to laboratory wildtype N2. **(D)** Developmental

710 rate analysis of mtDNA^{uaDf5} compared to laboratory wildtype N2, counting how many hours it

711 takes for starved L1s to reach gravidity once plated on food. **(E)** Developmental rate analysis of
712 mtDNA^{uaDf5} compared to laboratory wildtype N2, staging worms 60 hours after synchronized,
713 staved L1s are plated on food. **(F)** Survival curve analysis of mtDNA^{uaDf5} compared to laboratory
714 wildtype N2, day 1 is defined as the day starved L1s are plated on food. Median lifespan and
715 statistics are presented in Supplemental Figure 2. For **B-E**, box plots show median and IQR, and
716 the diamond indicates the mean. Statistical analysis was performed using the Mann-Whitney
717 test. (*** $p < 0.001$, n.s. not significant).
718

719 **Figure 2**

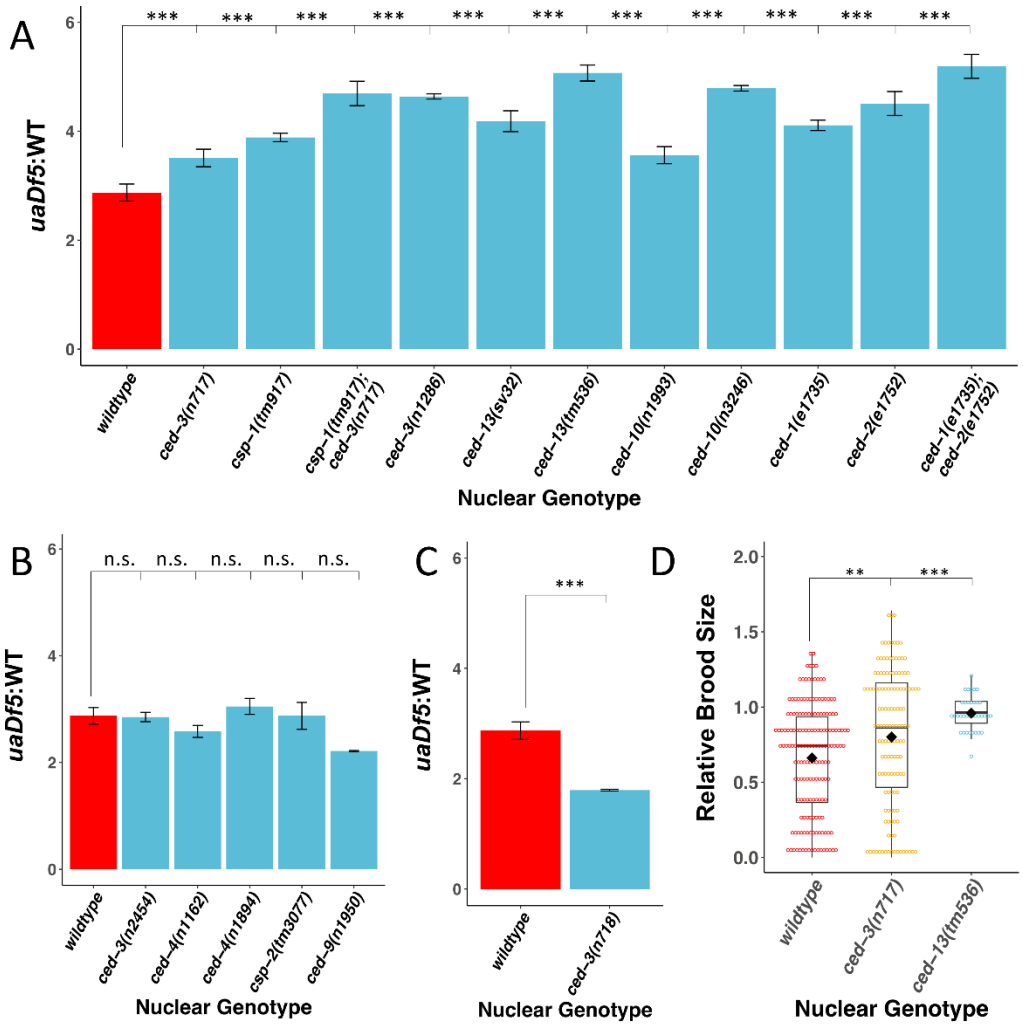

720
721

722 **Figure 2: Regulators of PCD act on mutant mtDNA. (A-C)** ddPCR analysis of the steady-state

723 molar ratio of mtDNA^{uaDf5} in 200 worm populations of day 1 adults of various PCD mutant

724 backgrounds. **(A)** PCD mutants that result in a significant increase in the molar ratio of

725 mtDNA^{uaDf5}. **(B)** PCD mutants that result in no statistical change in the molar ratio of mtDNA^{uaDf5}.

726 **(C)** PCD mutant that results in a significant decrease in the molar ratio of mtDNA^{uaDf5}. **(D)** The

727 relative brood size of the animals with and without mtDNA^{uaDf5} in the indicated mutant

728 backgrounds. Box plots show the median and IQR, the diamond indicates the mean. For **A-C**, n=3

729 or more biological replicates of 200 worm populations were performed for each genotype.
730 Statistical analysis was performed using one-way ANOVA with Dunnett's correction for multiple
731 comparisons. For **D**, statistical analysis was performed using the Mann-Whitney test. Error bars
732 represent SEM. (*** $p < 0.001$, ** $p < 0.01$, * $p < 0.05$, . $p < 0.1$, n.s. not significant).
733

734 **Figure 3**

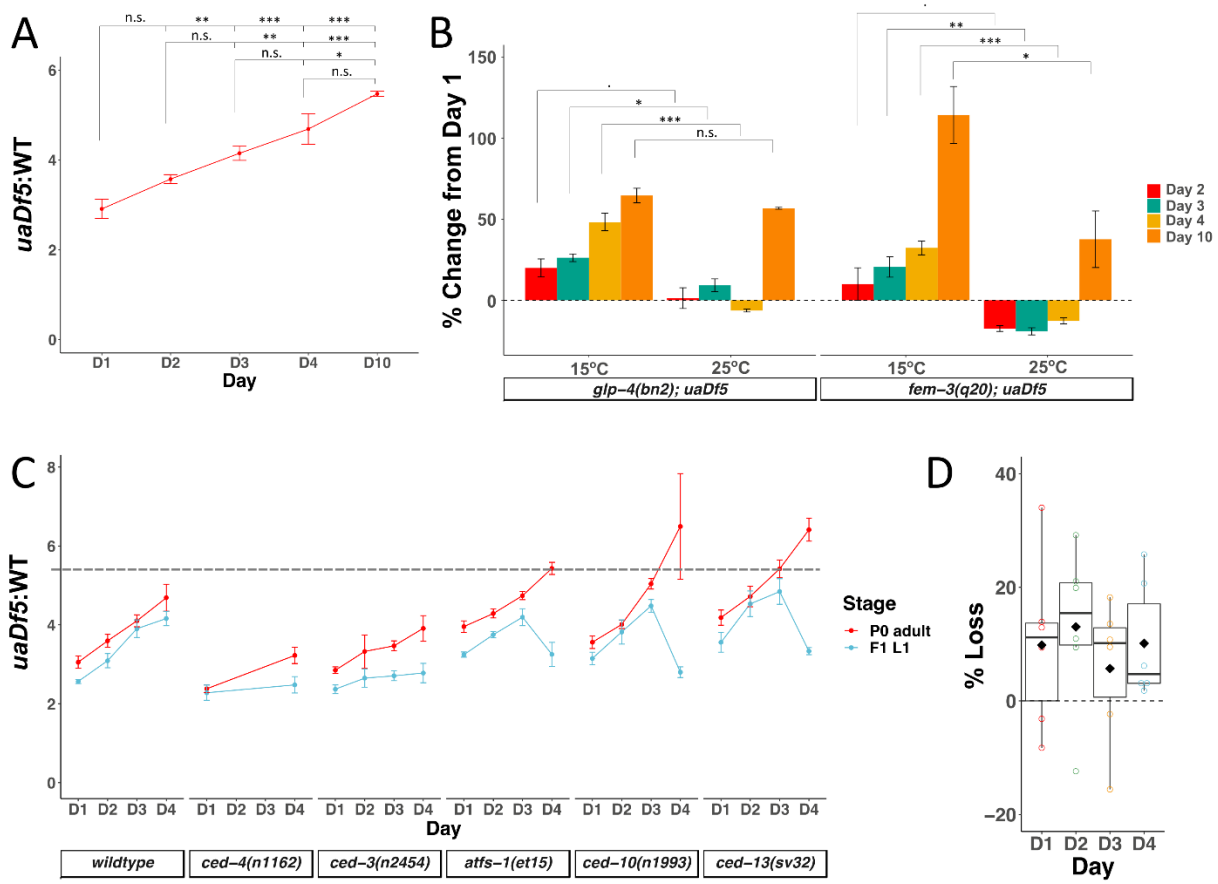

735

736 **Figure 3: mtDNA^{uaDf5} accumulates in the germline of aging adults, and evidence of purifying**

737 **selection between mother and offspring. (A)** Analysis of the molar ratio of mtDNA^{uaDf5} in aging

738 adults in a wildtype nuclear background. **(B)** Analysis of the percent change of *uaDf5:*WT from

739 day 1 (Y axis = (*uaDf5:*WT day x -*uaDf5:*WT day 1)/(*uaDf5:*WT day 1)). For *glp-1(q231ts), fem-*

740 *3(q20ts),* and *glp-4(bn2ts),* 15°C is the permissive temperature (germline development occurs)

741 and 25°C is the restrictive temperature (female germline development is inhibited). Statistical

742 analysis was performed using one-way ANOVA with Tukey correction for multiple comparisons.

743 (*** $p < 0.001$, ** $p < 0.01$, * $p < 0.05$, . $p < 0.1$). Error bars represent SEM. **(C)** Analysis of the

744 molar ratio of mtDNA^{uaDf5} in aging adults (P0 adult) and their L1 progeny (F1 L1) in various nuclear

745 backgrounds shows that all strains decrease the *uaDf5* load during transmission from mother to

746 offspring, and that strains with significantly higher mtDNA^{uaDf5} levels (*atfs-1(et15), ced-*
747 *10(n1993)*, and *ced-13(sv32)*) have a more significant removal mechanism at day 4 of adulthood.
748 n=3 or more replicates of 200 worm populations were performed for each timepoint. Error bars
749 represent SEM. Grey dashed line indicates a hypothetical threshold at which high mtDNA^{uaDf5}
750 burden activates enhanced intergenerational purifying selection in older mothers. **(D)** Analysis
751 of the measured loss of mtDNA^{uaDf5} between mother and offspring at each day of adulthood
752 shows that mtDNA^{uaDf5} removal occurs. n=6 replicates of 200 worm populations for each
753 condition.
754

755 **Figure 4**

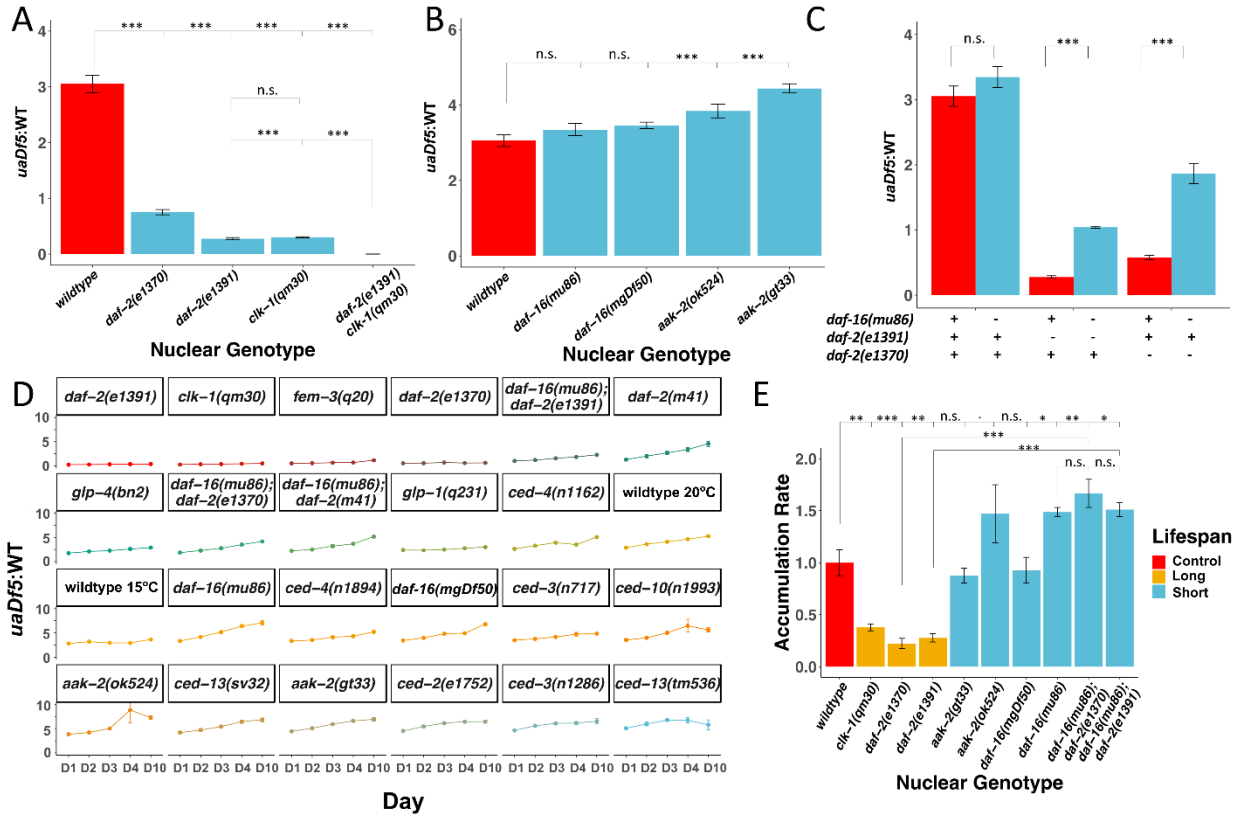

756

757 **Figure 4: Lifespan mutants have both a lower steady-state level and accumulation rate of**

758 **mtDNA^{uaDf5}. (A-C)** Analysis of molar ratio of mtDNA^{uaDf5} in day 1 adults of various mutant

759 backgrounds. **(A)** Analysis of steady-state mtDNA^{uaDf5} levels in long-lived mutants. **(B)** Analysis of

760 steady-state mtDNA^{uaDf5} levels in short-lived mutants, showing synergistic activity on mtDNA^{uaDf5}

761 removal capacity in the *daf-2(e1391) clk-1(qm30)* double mutant. **(C)** Analysis of steady-state

762 mtDNA^{uaDf5} levels in *daf-2(-)* single and *daf-16(-); daf-2(-)* double mutants, showing a partial

763 rescue of *daf-2(-)* phenotype by *daf-16(-)*. **(D)** Analysis of the molar ratio of mtDNA^{uaDf5} in aging

764 adults in 24 different nuclear backgrounds shows a consistent accumulation trend. **(E)** Summary

765 of the rate of increase for the lifespan regulation mutants, showing that *daf-16* rescues the *daf-*

766 *2* accumulation rate phenotype. The normalized accumulation rate was calculated by fitting a

767 regression line for each trial and then dividing the slope of the regression line by the slope of the

768 averaged regression line found in a wildtype background. For **all**, n=3 or more replicates of 200
769 worm populations for each genotype and stage. For **A and E,** statistical analysis was performed
770 using one-way ANOVA with Tukey correction for multiple comparisons. For **C**, statistical analysis
771 was performed using one-way ANOVA. For **B**, statistical analysis was performed using one-way
772 ANOVA with Dunnett's correction for multiple comparisons. Error bars represent SEM. (*** $p < 0.001$, ** $p < 0.01$, * $p < 0.05$, . $p < 0.1$, n.s. not significant).
773
774

775 **Figure 5**

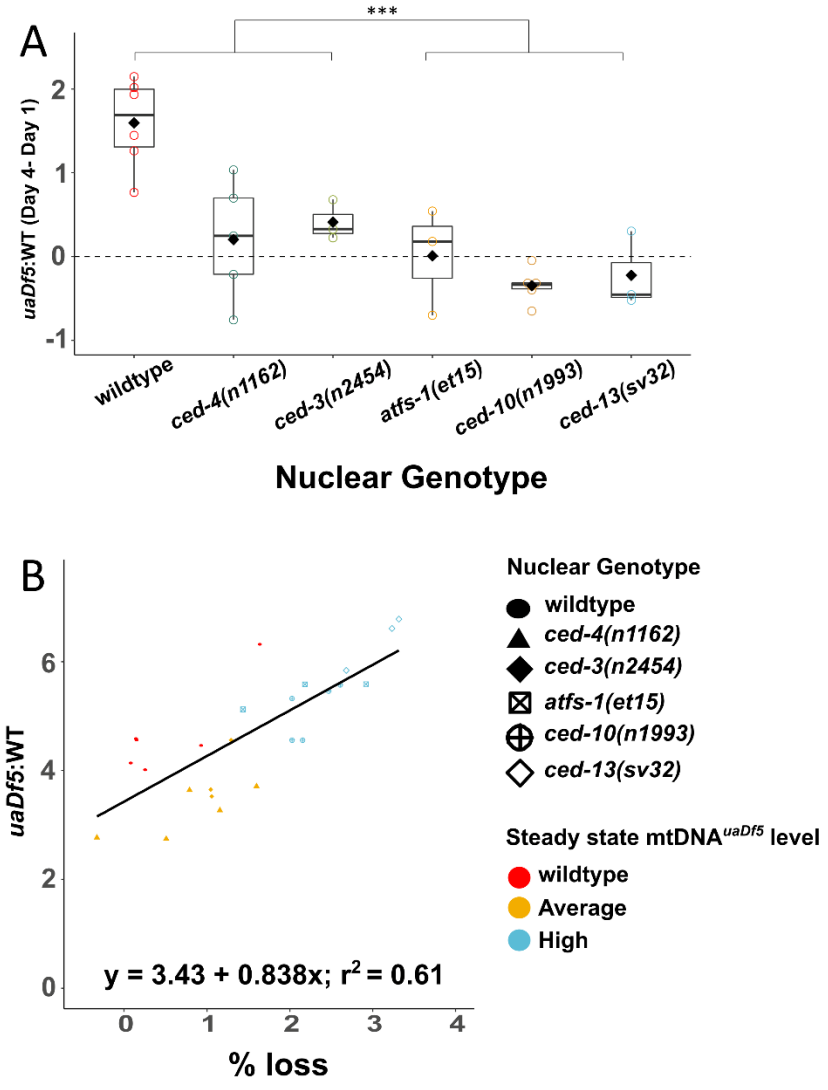

776

777 **Figure 5: Evidence for late adulthood-specific mechanisms for removal of mtDNA^{uaDf5}**

778 **(A)** Subtracting *uaDf5:*WT in progeny from day 1 adults from progeny of day 4 adults shows that

779 day 4 F1-L1s tend to have higher mtDNA^{uaDf5} burden than their day 1 siblings, but this is no longer

780 the case in nuclear backgrounds that result in a significantly higher steady-state levels of

781 mtDNA^{uaDf5} in the adult. n=3 or more replicates for each genotype and statistical analysis was

782 performed using the Mann-Whitney test. **(B)** Comparison of the molar ratio of mtDNA^{uaDf5} in day

783 4 adult mothers to the absolute % removal of mtDNA^{uaDf5} from mother to offspring shows a

784 positive correlation. (*** $p < 0.001$).

785
786

787 **Figure 6**

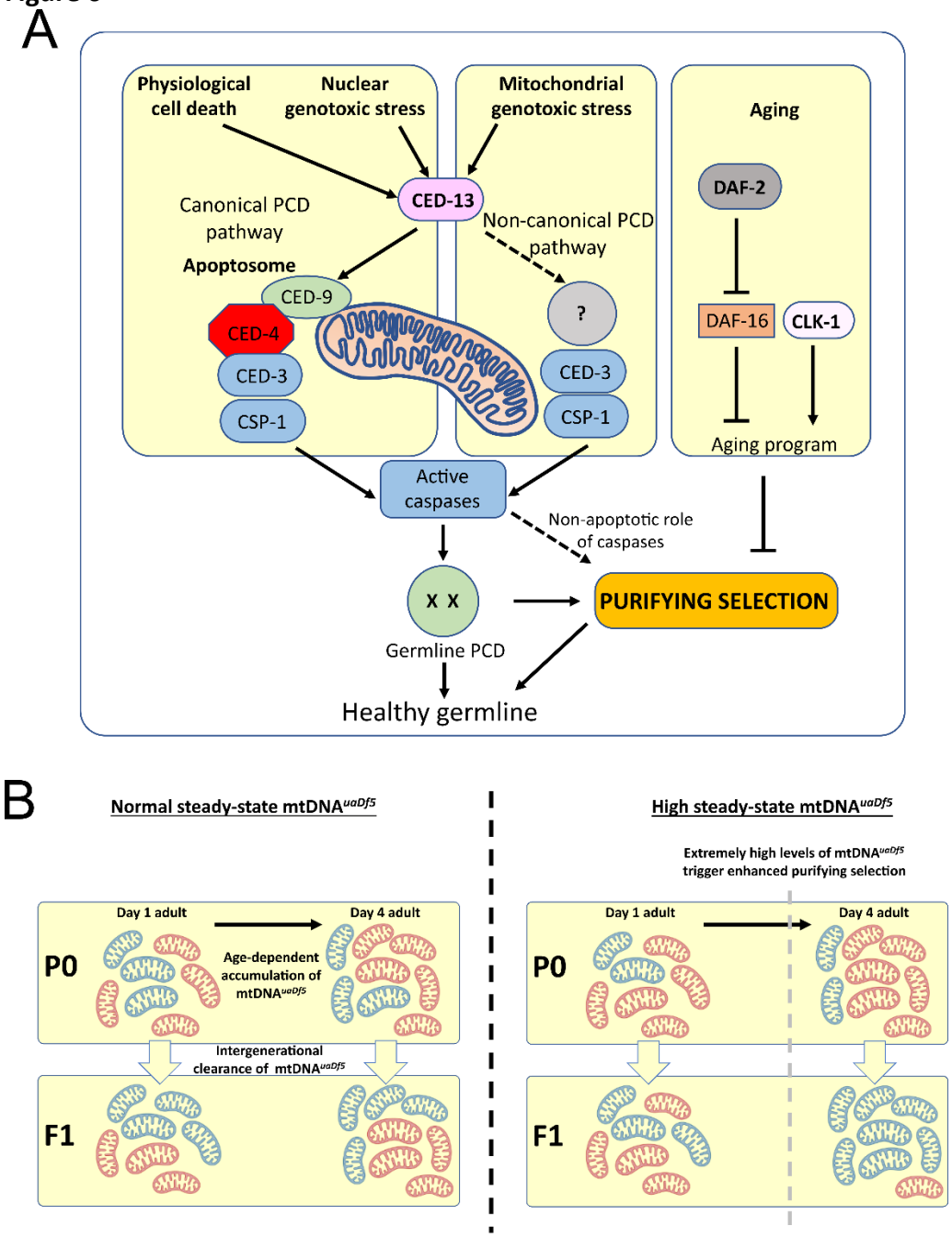

788

789 **Figure 6: Regulation of mtDNA^{uaDf5} accumulation and transmission by the PCD and aging**

790 **pathways**

791 **(A)** Our results suggest that CED-3 and CSP-1, which are activated by BH-3 only protein CED-13,

792 function cooperatively to promote mitochondrial purifying selection, independent of CED-9 and

793 the CED-4 apoptosome. The clearance of mtDNA^{uaDf5} may therefore involve induction of a non-
794 canonical germline PCD mechanism or non-apoptotic action of the CED-13/caspase axis.
795 Additionally, IIS and CLK-1 aging pathways, act synergistically to regulate mitochondrial purifying
796 selection**. (B)** mtDNA^{uaDf5} (red) accumulates in the germline relative to mtDNA^{WT} (blue) as adults
797 age and the increased mtDNA^{uaDf5} levels are transmitted to the progeny, although the mtDNA^{uaDf5}
798 burden is consistently lower in progeny than mothers. This intergenerational purifying selection
799 is enhanced in the older mothers of mutants with high steady-state mtDNA^{uaDf5} (e.g., *ced-13*, *ced-*
800 *10,* and *atfs-1*), suggesting a threshold beyond which a germline PCD-independent mtDNA quality
801 control process may be initiated or enhanced in these older mothers.

802 **Supplemental Materials**

803 **Supplemental Figure 1**

A

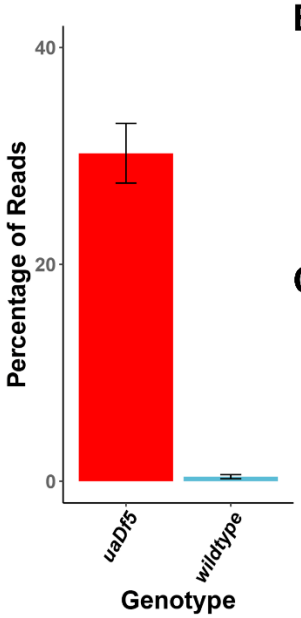

B

Sample	Allele	Total reads	Variant reads	% variant
A	*uaDf5*	858.40*	658.48*	76.71
	w47	631	472	72.62
B	*uaDf5*	451.54*	347.51*	76.96
	w47	339	248	71.06

C

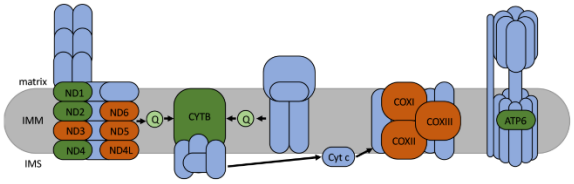

Complex:	I	II	III	IV	V
nDNA-encoded	~30	~8	4	~6	~13
mtDNA-encoded	7	1	0	3	1

D

ND4 (wildtype)

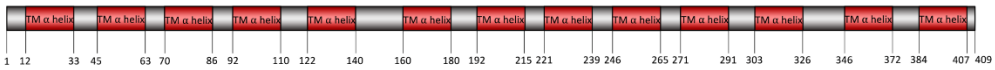

ND4 (*w47*)

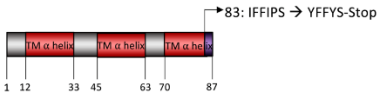

E

ND1 (wildtype)

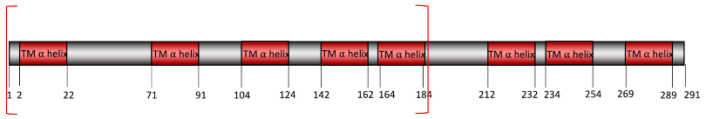

CYTB (wildtype)

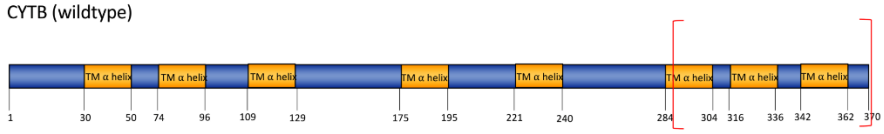

ND1-CYTB (*uaDf5*)

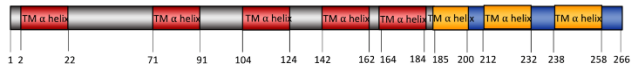

804

805 **Supplemental Figure 1: Characterization of the *uaDf5* allele. (A)** The percentage of reads that
806 mapped to the *w47* deletion in *uaDf5* samples (red) and wildtype samples (blue). Error bars
807 represent SEM. **(B)** Table outlining the percentage of reads that mapped to the *w47* and *uaDf5*
808 deletions in *uaDf5* samples. The number of variant reads was determined by averaging the
809 mapped reads across the deleted region and subtracting that from the average number of reads
810 mapped to the rest of the mtDNA genome (total reads). **(C)** Diagram showing the mitochondrial
811 respiratory chain (MRC) machinery subunits. Blue indicates nDNA-encoded subunits, orange and
812 green indicate mtDNA-encoded subunits. Green indicates those subunits that are knocked out in
813 the *uaDf5* allele (including ND4 which is knocked out by the linked *w47* mutation). **(D)** Diagram
814 showing the likely effect of the *w47* mutation on ND4 protein translation. ND4 is a 409-aa long
815 transmembrane subunit that spans the inner mitochondrial membrane 13 times. The *w47*
816 mutation results in a premature stop codon at position 89, eliminating 10 of the 13 alpha-helix
817 membrane domains. **(E)** Diagram showing the likely effect of the *uaDf5* mutation on ND1 protein
818 translation. ND1 is a 291-aa long transmembrane subunit that spans the inner mitochondrial
819 membrane 8 times and CYTB is a 370-aa long transmembrane subunit that spans the inner
820 mitochondrial membrane 8 times. The *uaDf5* mutation results in a 266 amino acid long fusion
821 protein that connects the first 185 amino acids (and 5 subunits) of ND1 with the last 81 amino
822 acids (and 3 subunits) of CYTB.
823

824 **Supplemental Figure 2**

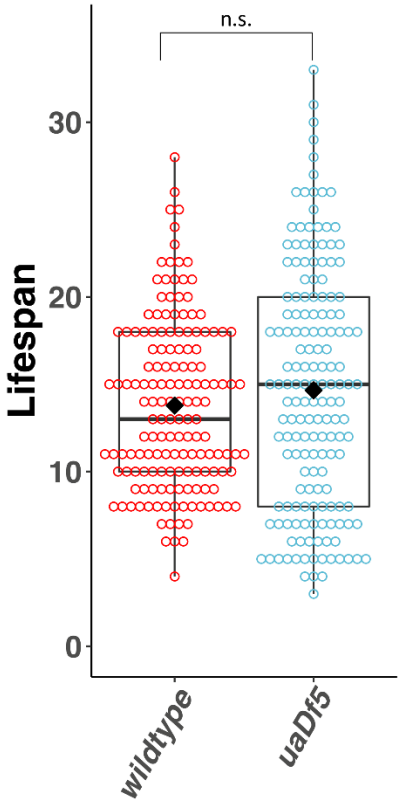

825

826 **Supplemental Figure 2: Lifespan analysis of the impact of *uaDf5*.** Lifespan analysis of N2 bearing

827 *uaDf5* compared to wildtype N2. Day 1 is defined as the day starved L1s are plated on food. Box

828 plots show median and IQR, and the diamond indicates the mean. Statistical analysis was

829 performed using the Mann-Whitney test. (n.s. not significant).

830

831 **Supplemental Figure 3**

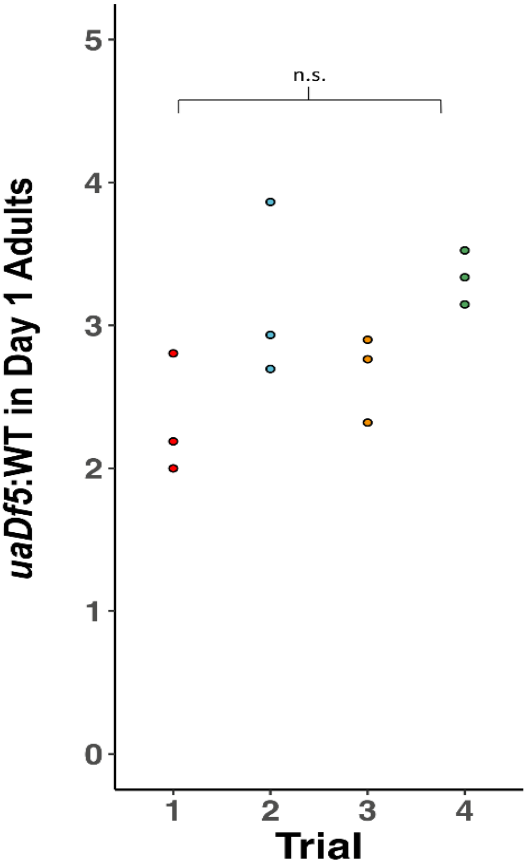

832

833 **Supplemental Figure 3: Reproducibility of ddPCR measurement of *uaDf5*.** Analysis of the steady-
834 state of *uaDf5* in a wildtype nuclear background shows highly stable steady-state levels. Trials
835 were done months apart on different thaws. Dots represent biological replicates. Statistical
836 analysis was performed using one-way ANOVA with Tukey correction for multiple comparisons.
837 (n.s. not significant).

838

839 **Supplemental Figure 4**

A

Allele	Location	Domain	Level of *uaDf5*
n1286	W428opal	p15	highest
n717	Position 403 - Exon 7 acceptor	p15	high
n2454	A466T	p15	unchanged
n718	G65R	Prodomain	low

B

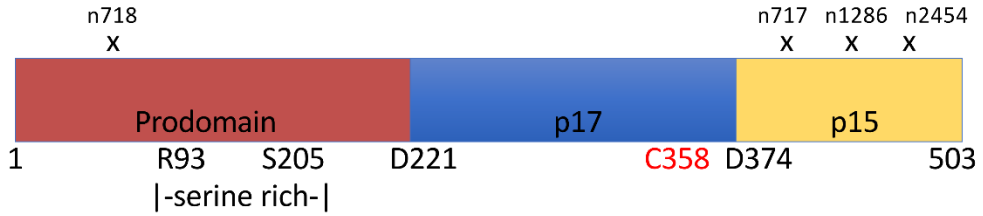

840

841 **Supplemental Figure 4: Analysis of the *ced-3* alleles. (A)** Locations and consequences of the four

842 tested *ced-3* alleles, as well as the measured fractional abundance of *uaDf5*. **(B)** Diagram showing

843 the locations of the mutations for each allele.

844

845 **Supplemental Figure 5**

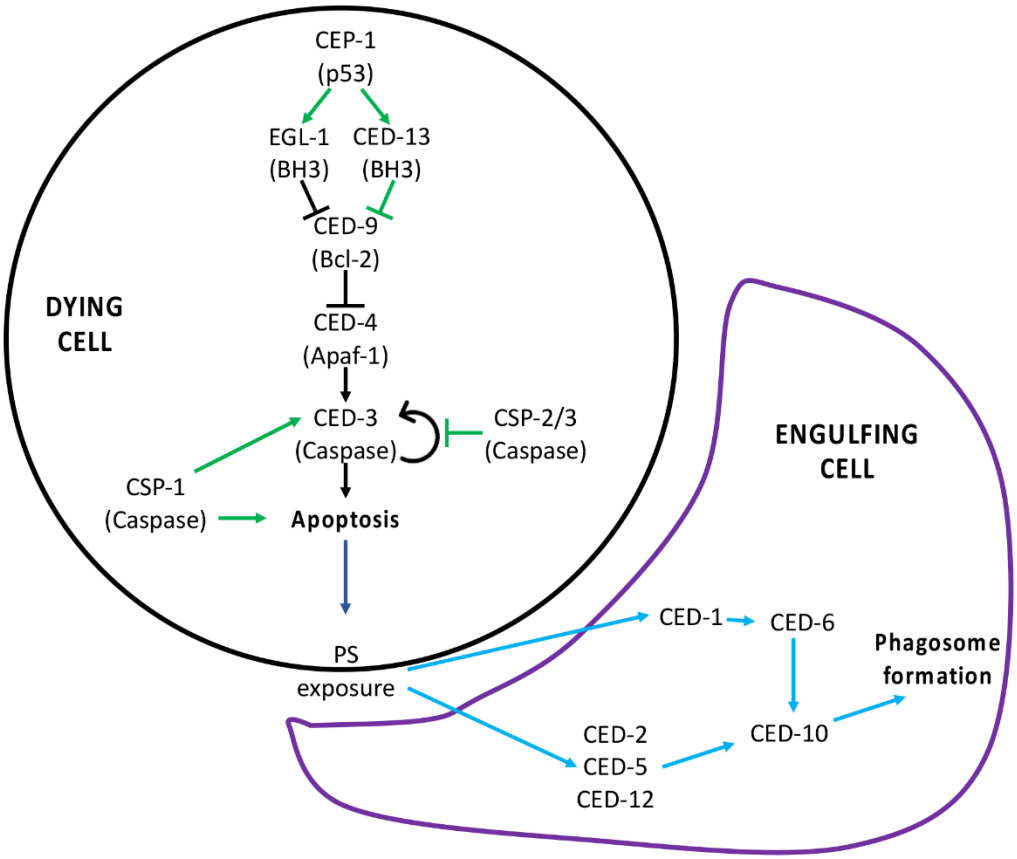

846

847

848 **Supplemental Figure 5: PCD Signaling pathway. (A)** Signaling pathway for programmed cell

849 death. The canonical pathway is shown with black arrows, the noncanonical pathway is shown

850 with green arrows, and the downstream engulfment pathway is shown with blue arrows.

851 Adapted from [38].

852

853 **Supplemental Figure 6**

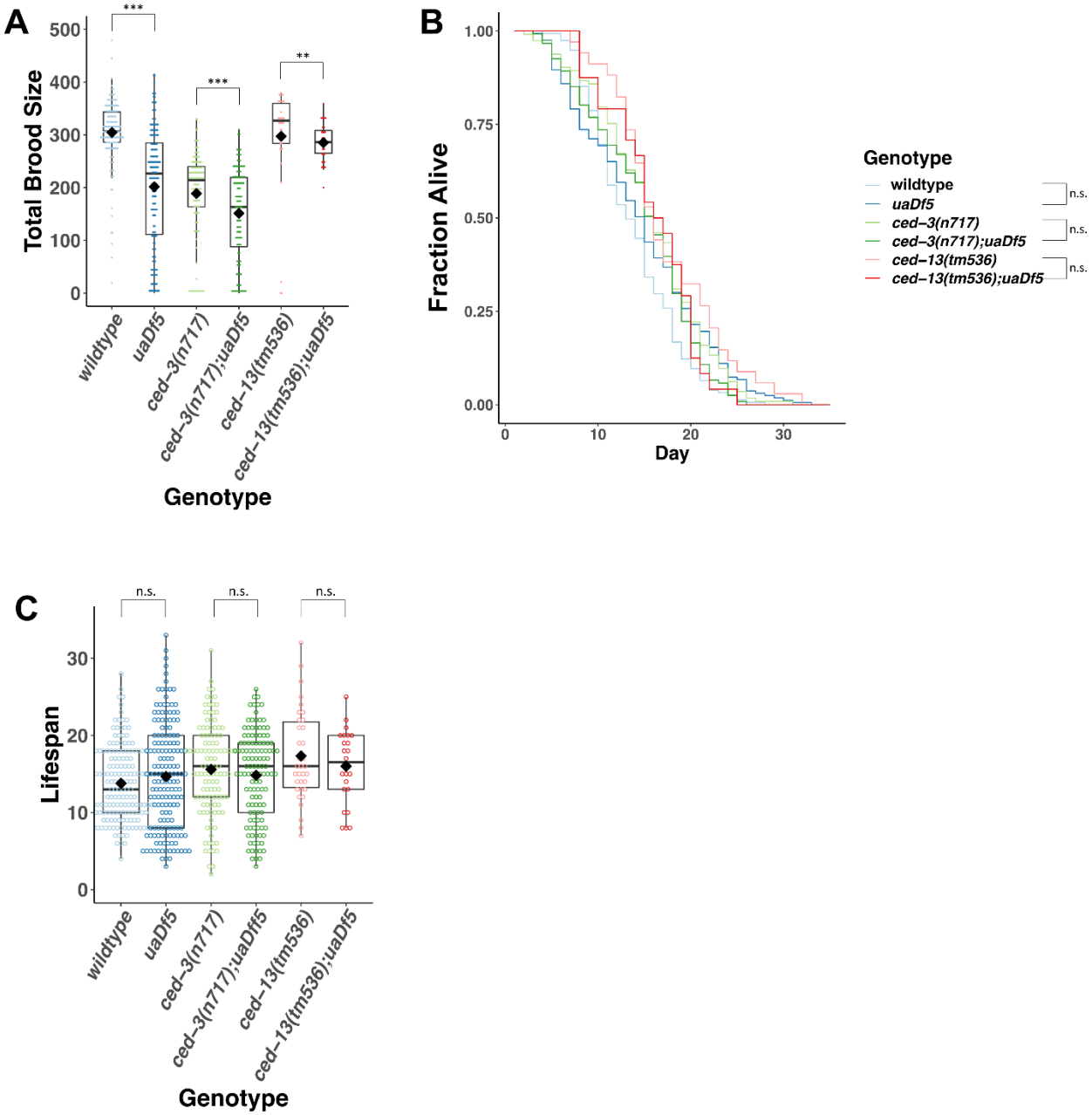

854

855 **Supplemental Figure 6: Analysis of the impact of *uaDf5* on fitness parameters in PCD mutants.**

856 **(A)** Brood size analysis of PCD mutants. **(B)** Lifespan analysis shows that *uaDf5* does not affect

857 lifespan in both wildtype background and in PCD mutant backgrounds. **(C)** Lifespan analysis

858 shows that *uaDf5* does not affect lifespan in a wildtype nuclear background nor in PCD mutant

859 backgrounds. For **B and C,** day 1 is defined as the day starved L1s are plated on food. For **A and**

860 **C**, box plots show median and IQR, and the diamond indicates the mean. Statistical analysis was

861 performed using the Mann-Whitney Wilcoxon test. (*** $p < 0.001$, ** $p < 0.01$, * $p < 0.05$, . $p <$

862 0.1, n.s. not significant).

863

864

865 **Supplemental Figure 7**

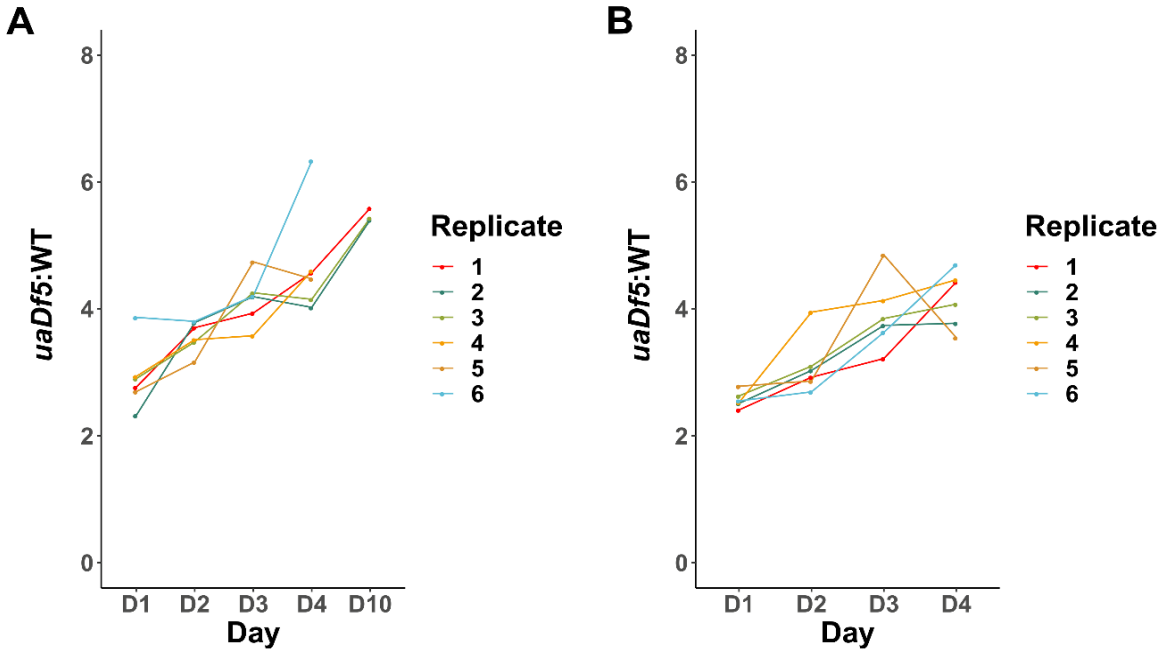

866

867 **Supplemental Figure 7: *uaDf5* accumulation in individual lines of adults and progeny. (A)**
868 Analysis of *uaDf5* accumulation in individual lines of aging P0 adults shows a consistent
869 accumulation trend as adults age. **(B)** Analysis of *uaDf5* accumulation in individual lines of F1-L1
870 progeny that were born from those mothers shown in panel A show a consistent trend of progeny
871 born from older mothers inheriting a larger *uaDf5* load than their siblings born from younger
872 mothers.

873

874 **Supplemental Figure 8**

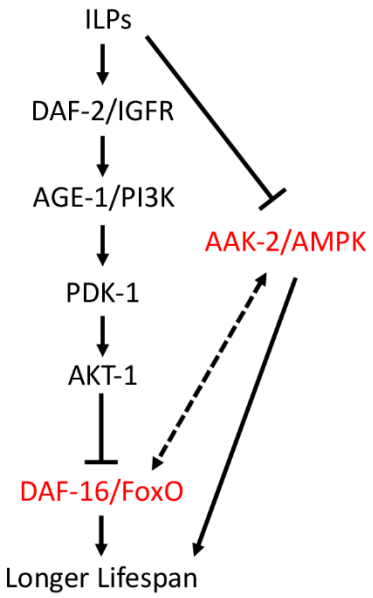

875

876 **Supplemental Figure 8: IIS Signaling pathway.** Insulin-like peptides (ILPs) bind to DAF-2 and

877 activate the PI3P pathway which prevents nuclear translocation of DAF-16. AAK-2 may

878 phosphorylate and activate DAF-16 transcriptional activity. Loss of *aak-2* or *daf-2* (highlighted in

879 red) reduces lifespan

880

881 **Supplemental Figure 9**

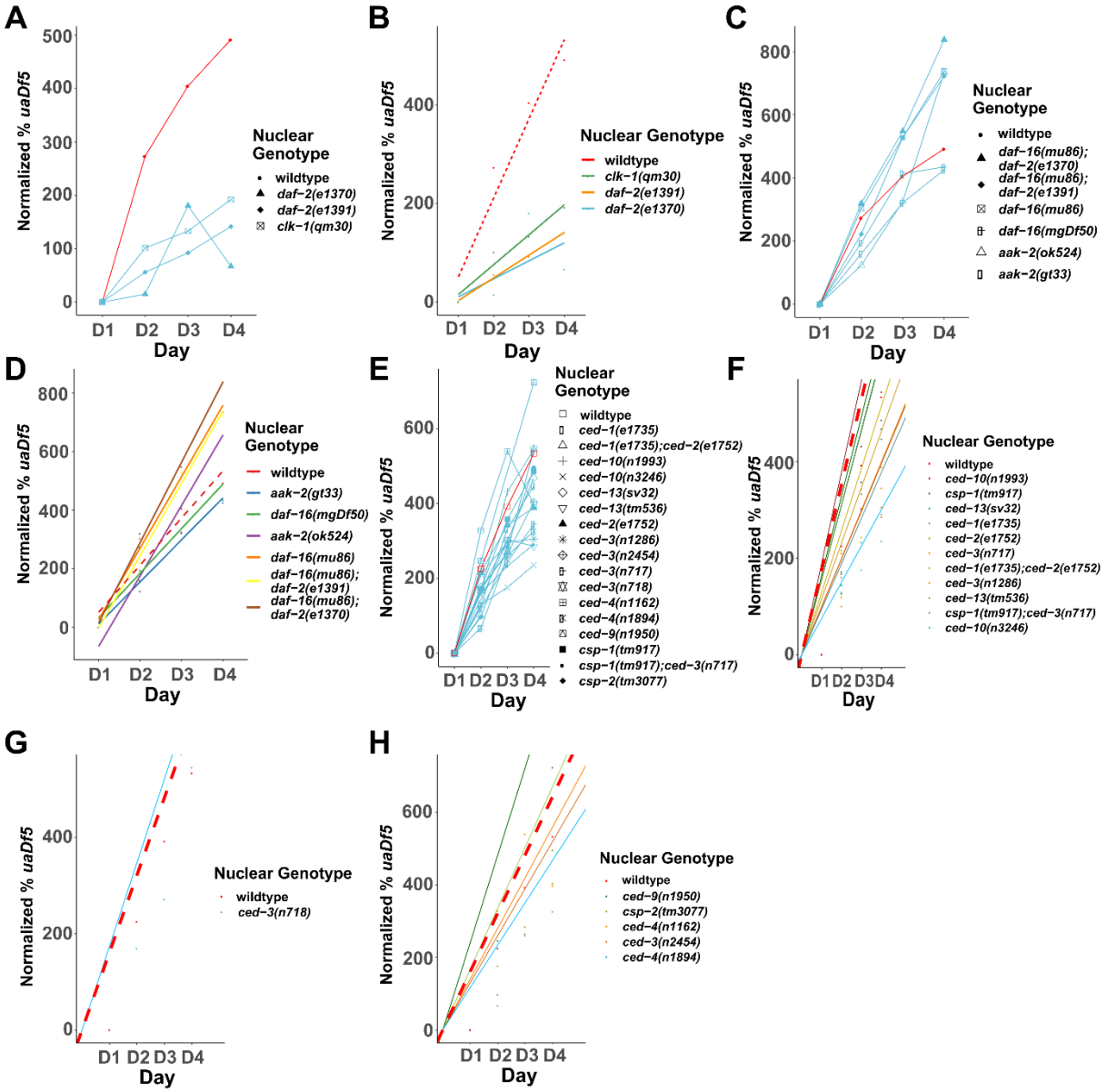

882

883 **Supplemental Figure 9: Analysis of the accumulation of mtDNA^{uaDf5} in PCD and lifespan**

884 **mutants.** Analysis of the normalized fractional abundance *uaDf5* [(% *uaDf5* day x- % *uaDf5* day

885 1)* % *uaDf5* day 1] in steady-state populations, showing the accumulation rate of mtDNA^{uaDf5} as

886 worms age from day 1 to day 4 of adulthood. **(A)** Analysis of the accumulation of *uaDf5* in long-

887 lived mutants. **(B)** Analysis of the accumulation of mtDNA^{uaDf5} in short-lived mutants. **(C-D)** Linear

888 regression analysis of the normalized fractional abundance *uaDf5* [(% *uaDf5* day x- % *uaDf5* day
889 1)* % *uaDf5* day 1] in steady-state populations, showing the accumulation rate of mtDNA^{uaDf5} as
890 worms age from day 1 to day 4 of adulthood. **(C)** Analysis of long-lived mutants. **(D)** Analysis of
891 short-lived mutants. **(E)** Analysis of the accumulation of mtDNA^{uaDf5} in PCD mutants. **(F-H)** Linear
892 regression analysis of the normalized fractional abundance mtDNA^{uaDf5} [(% *uaDf5* day x- % *uaDf5*
893 day 1)* % *uaDf5* day 1] in steady-state populations, showing the accumulation rate of mtDNA^{uaDf5}
894 as worms age from day 1 to day 4 of adulthood. **(F)** Analysis of PCD mutants with significantly
895 high steady-state level of mtDNA^{uaDf5}. **(G)** Analysis of PCD mutants with significantly low steady-
896 state level of mtDNA^{uaDf5}. **(H)** Analysis of PCD mutants with no significant change in the steady-
897 state level of mtDNA$^{uaDf5.}$ For **C, D, F, G, and H** dots represent actual datapoints, lines are fitted
898 regression models of the data. For all, n=3 replicates or more of 200 worm populations for each
899 datapoint.
900
901

902 **Supplemental Figure 10**

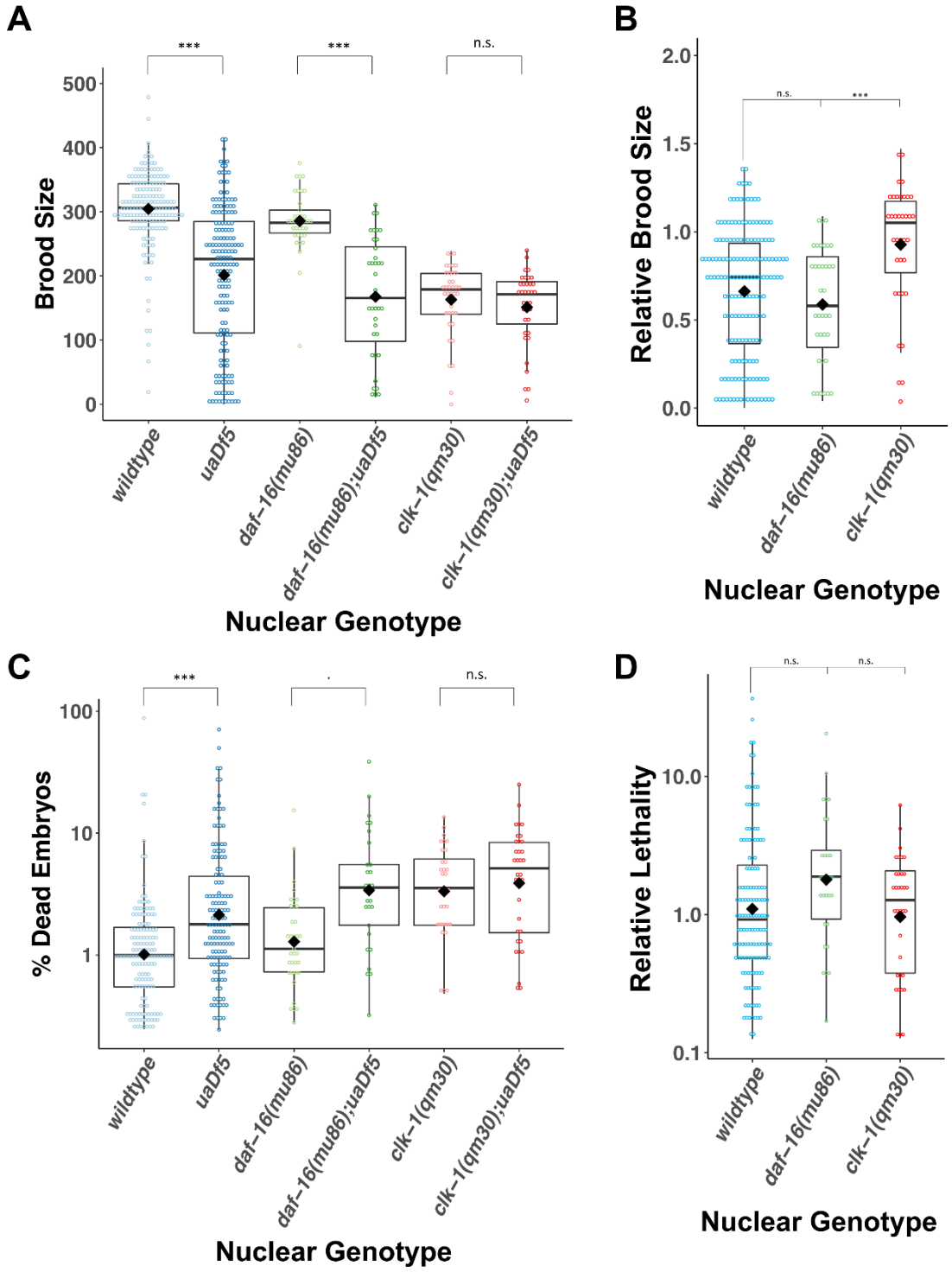

903

904 **Supplemental Figure 10: *uaDf5* differentially impacts fitness parameters in lifespan-affecting**

905 **mutants. (A-B)** Brood size analysis showing how *uaDf5* differentially impacts brood size in

906 lifespan mutant backgrounds. *uaDf5* has no negative impact on the long-lived mutant *clk-1* but
907 has a modestly larger negative impact on the short-lived mutant *daf-16* than it does in the
908 wildtype background. **(B)** Relative brood size of the animals with and without *uaDf5* in the
909 indicated mutant backgrounds. **(C-D)** Embryonic lethality analysis showing how *uaDf5*
910 differentially impacts embryonic lethality in lifespan mutant backgrounds. *uaDf5* has no negative
911 impact on the long-lived mutant *clk-1* but has a modestly larger negative impact on the short-
912 lived mutant *daf-16* than it does in a wildtype background. **(D)** Relative lethality of the animals
913 with and without *uaDf5* in the indicated mutant backgrounds. Box plots show median and IQR,
914 and the diamond indicates the mean. For **A and C**, statistical analysis was performed using the
915 Mann-Whitney test. For **B and D**, statistical analysis was performed using the Kruskal-Wallis test.
916 (*** $p < 0.001$, ** $p < 0.01$, * $p < 0.05$, . $p < 0.1$, n.s. not significant).
917

918 **Supplementary Table 1:** A summary of all mutants analyzed in the PCD pathway, including their
919 known homologs, whether they are part of the core PCD machinery, if they are pro-apoptotic or
920 anti-apoptotic, whether they are mitochondrial proteins, and molecular details of the alleles
921 analyzed.

Gene	Homolog	Core Machinery	Role in Apoptosis	Mitochondrial?	Allele	Parental Strain	Molecular Nature of the Allele	Protein Change
ced-1	SCARF2	N	Pro(engulfment)	N	*e1735*	CB3203	Substitution	Nonsense Q→Ochre
ced-2	CRK	N	Pro(engulfment)	N	*e1752*	CB3257	Substitution	Nonsense W→Opal
ced-3	CASPASE	Y	Pro(executor caspase)	N	*n717*	MT1522	Substitution	Splice site C→T
					n1286	MT3002	Substitution	Nonsense W→Opal
					n718	MT1743	Substitution	Missense G→R
					n2454	MT8354	Substitution	Missense A→T
ced-4	APAF1	Y	Pro(apoptosome)	Y/N (primarily nuclear membrane)	*n1162*	MT2547	Substitution	Nonsense Q→Ochre
					n1894	MT5287	Not curated	Unknown
ced-9	BCL2	Y	Anti	Y	*n1950*	MT4770	Substitution	Missense G→E
ced-10	RAC	N	Pro(engulfment)	N	*n1993*	MT5013	Substitution	Missense V→G
					n3246	MT9958	Substitution	Missense G→R
ced-13	BH3	N	Pro	N	*tm536*	FX536	523bp deletion	Only first 17bp remain
					sv32	MD792	1304bp deletion	Complete knockout, also *inx-5*
csp-1	CASPASE	N	Pro(caspase)	N	*tm917*	JR3196	751bp deletion	Only first 59bp remain
csp-2	CASPASE	N	Anti	N	*tm3077*	JR3397	319bp deletion	Start at position 7317, deletes parts of exon 13

								and all of 14

924 **Supplementary Table 2:** A summary of all lifespan mutants analyzed, including their known

925 homologs, cellular pathways they are known to act in, whether the mutant extends or reduces

926 lifespan, and molecular details of the alleles analyzed.

Gene	Homologs	Pathway	Allele	Parental Strain	Molecular Nature of the Allele	Protein Change	Mutant lifespan	Note
aak-2	AMPK	IIS pathway, adult lifespan, peptidyl-serine phosphorylation, regulation of protein localization	*gt33*	TG38	606bp deletion	Starts at position 3979, deletes exon 3	Decrease	-
			ok524	RB754	408bp deletion	Starts at position 4136, deletes part of exon 3	Decrease	-
clk-1	COQ7	Adult behavior, regulation of cellular metabolism	*qm30*	MQ130	590bp deletion	Starts at position 1044, deletes part of exon 4 and 5	Increase	-
daf-2	IGFR	IIS pathway, cellular response to salt, negative regulator of macromolecule metabolic processes, positive regulation of developmental growth	*e1391*	DR1574	Substitution	Missense P→L	Increase	ts
			e1370	CB1370	Substitution	Missense P→S	Increase	ts
			m41	DR1564	Substitution	Missense G→E	Increase	ts
daf-16	FOXO	IIS pathway, defense response to bacterium, regulation of cellular biosynthetic process, regulation of post-	*mu86*	CF1038	1098bp deletion	Deletes 5 exons	Decrease	-
			mgDf50	GR1307	20193bp deletion with TCTTCATTTTCAG insertion	Deletes 7 exons	Decrease	-

		embryonic development						
fem-3	novel	Male somatic sex determination, masculinization of hermaphrodite germline, positive regulation of macromolecule metabolic process	*q20*	JK816	Not curated	Unknown	Increase	Gof and ts; female germline development inhibited
glp-4	VARS	Cell fate specification, embryonic pattern specification, positive regulation of cell proliferation	*bn2*	SS104	Substitution	Missense G→D	Increase	ts; germline development inhibited

927
928

929 **Supplementary Table 3:** *C. elegans* strains used in this study.

Strain	Genotype	Source
N2	wildtype	CGC
LB138	*him-8(e1489) IV; uaDf5/+*	CGC
JR3630	*N2; uaDf5/+ (8x backcross version of LB138, him(e1489) was outcrossed)*	This study
JR3792	*ced-3(n717) IV; uaDf5/+* (line 1)	This study
JR3880	*ced-3(n717) IV; uaDf5/+ (*line 2)	This study
JR4330	*csp-1(tm917) II; uaDf5/+* (line 1)	This study
JR4331	*csp-1(tm917) II; uaDf5/+* (line 2)	This study
JR3977	*ced-3(n1286) IV; uaDf5/+*	This study
JR3955	*ced-13(sv32) X; uaDf5/+* (line 1)	This study
JR3956	*ced-13(sv32) X; uaDf5/+* (line 2)	This study
JR3976	*ced-13(tm536) X; uaDf5/+*	This study
JR3926	*ced-10(n1993) IV; uaDf5/+* (line 1)	This study
JR3927	*ced-10(n1993) IV; uaDf5/+* (line 2)	This study
JR3928	*ced-10(n1993) IV; uaDf5* (line 3)	This study
JR4001	*ced-10(n3246) IV; uaDf5/+* (line 1)	This study
JR4002	*ced-10(n3246) IV; uaDf5/+* (line 1)	This study
JR3972	*ced-1(e1735) I; uaDf5/+* (line 1)	This study
JR3973	*ced-1(e1735) I; uaDf5/+* (line 2)	This study
JR3978	*ced-2(e1752) IV; uaDf5/+*	This study
JR4010	*ced-1(e1735)I; ced-2(e1752)IV; uaDf5/+*	This study
JR3938	*ced-3(n2454) IV; uaDf5/+*	This study
JR3925	*ced-4(n1162) III; uaDf5/+* (line 1)	This study
JR4017	*ced-4(n1894) III; uaDf5/+* (line 2)	This study
JR3986	*csp-2(tm3077) IV; uaDf5/+* (line 1)	This study
JR3987	*csp-2(tm3077) IV; uaDf5/+* (line 1)	This study
JR4027	*ced-9(n1950) III; uaDf5/+*	This study
JR3983	*ced-3(n718) IV; uaDf5/+* (line 1)	This study
JR3984	*ced-3(n718) IV; uaDf5/+* (line 2)	This study
MT1522	*ced-3(n717) IV*	CGC
FX536	*ced-13(tm536) X*	CGC
JR3965	*glp-4(bn2) I; uaDf5/+* (line 1)	This study
JR3966	*glp-4(bn2) I; uaDf5/+* (line 2)	This study
JR3949	*fem-3(q20) IV; uaDf5/+*	This study
JR3937	*atfs-1(et15) V; uaDf5/+*	This study
JR3959	*daf-2(e1370) III; uaDf5/+* (line 1)	This study
JR3960	*daf-2(e1370) III; uaDf5/+* (line 2)	This study
JR3963	*daf-2(e1391) III; uaDf5/+* (line 1)	This study
JR3964	*daf-2(e1391) III; uaDf5/+* (line 2)	This study

JR3992	*clk-1(qm30) III; uaDf5/+* (line1)	This study
JR3993	*clk-1(qm30) III; uaDf5/+* (line 2)	This study
JR4059	*daf-2(e1391) clk-1(qm30) III; uaDf5/+* (line 1)	This study
JR4060	*daf-2(e1391) clk-1(qm30) III; uaDf5/+* (line 2)	This study
JR3995	*daf-16(mu86) I; uaDf5/+* (line 1)	This study
JR3996	*daf-16(mu86) I; uaDf5/+* (line 2)	This study
JR3997	*daf-16(mgDf50) I; uaDf5/+* (line 1)	This study
JR3998	*daf-16(mgDf50) I; uaDf5/+* (line 2)	This study
JR4011	*aak-2(ok524) X; uaDf5/+*	This study
JR4012	*aak-2(gt33) X; uaDf5/+* (line 1)	This study
JR4013	*aak-2(gt33) X; uaDf5/+* (line 2)	This study
JR4008	*daf-16(mu86) I; daf-2(e1391) III; uaDf5/+* (line 1)	This study
JR4007	*daf-16(mu86) I; daf-2(e1391) III; uaDf5/+* (line 2)	This study
JR4005	*daf-16(mu86) I; daf-2(e1370) III; uaDf5/+* (line 1)	This study
JR4006	*daf-16(mu86) I; daf-2(e1370) III; uaDf5/+* (line 2)	This study
JR3948	*daf-2(m41) III; uaDf5/+*	This study
JR3941	*glp-1(q231) III; uaDf5/+* (line 1)	This study
JR3942	*glp-1(q231ts) III; uaDf5/+* (line 2)	This study
JR4024	*daf-16(mu86) I; daf-2(m41) III; uaDf5/+* (line 1)	This study
JR4025	*daf-16(mu86) I; daf-2(m41) III; uaDf5/+* (line 2)	This study
CF1038	*daf-16(mu86) I*	CGC
MQ130	*clk-1(qm30) III*	CGC
JR3981	*csp-1(tm917) II; ced-3(n717) IV; uaDf5/+* (line 1)	This study
JR3982	*csp-1(tm917); ced-3(n717) IV; uaDf5/+* (line 2)	This study

Acknowledgments

We would like to thank the members of the Rothman lab for their support. We thank Jen Smith and the BNL at UCSB for providing excellent facilities which were necessary for this work. We thank Kyle Ploense for his help in statistical analysis. Worm strains used in this work were provided by the Mitani lab, as well as the Caenorhabditis Genetics Center (CGC), which is funded by NIH Office of Research Infrastructure Programs Grant P40 OD010440.

Competing Interests

The authors declare no competing or financial interests.

Author contributions

Sagen E. Flowers - conceptualization, investigation, funding acquisition, writing – original draft preparation, writing – review and editing

Rushali Kothari – investigation, writing – review and editing

Yamila N. Torres Cleuren - investigation, writing – review and editing

Melissa R. Alcorn – statistics, writing – review and editing

Chee Kiang Ewe - writing – review and editing

Geneva Alok - writing – review and editing

Pradeep M. Joshi – conceptualization, investigation, writing – review and editing

Joel H. Rothman - conceptualization, supervision, funding acquisition, writing – review and editing

Funding

This work was supported by the grants from the National Institutes of Health (#R01HD082347, #R01HD081266, #R01GM143771, and #R21AG068915).

954 **Data Availability**

955 All data generated or analyzed during this study are included in this article and accompanied
956 supplementary materials.

957 **References**

958 1. YS N, DM T. Mitochondrial disease: genetics and management. J Neurol. J Neurol;
959 2016;263: 179–191. doi:10.1007/S00415-015-7884-3

960 2. PF C. Mitochondrial disease in adults: what's old and what's new? EMBO Mol Med.
961 EMBO Mol Med; 2015;7: 1503–1512. doi:10.15252/EMMM.201505079

962 3. Gorman GS, Schaefer AM, Ng Y, Gomez N, Blakely EL, Alston CL, et al. Prevalence of
963 nuclear and mitochondrial DNA mutations related to adult mitochondrial disease. Ann
964 Neurol. John Wiley & Sons, Ltd; 2015;77: 753–759. doi:10.1002/ANA.24362

965 4. Ghaoui R, Sue CM. Movement disorders in mitochondrial disease. J Neurol. Dr. Dietrich
966 Steinkopff Verlag GmbH and Co. KG; 2018;265: 1230–1240. doi:10.1007/s00415-017-
967 8722-6

968 5. Area-Gomez E, Schon EA. Mitochondrial genetics and disease. Journal of Child Neurology.
969 SAGE Publications Inc.; 2014. pp. 1208–1215. doi:10.1177/0883073814539561

970 6. Dhillon VS, Fenech M. Mutations that affect mitochondrial functions and their
971 association with neurodegenerative diseases. Mutation Research - Reviews in Mutation
972 Research. 2014. pp. 1–13. doi:10.1016/j.mrrev.2013.09.001

973 7. Park CB, Larsson NG. Mitochondrial DNA mutations in disease and aging. Journal of Cell
974 Biology. 2011. pp. 809–818. doi:10.1083/jcb.201010024

975 8. Burté F, Carelli V, Chinnery PF, Yu-Wai-Man P. Disturbed mitochondrial dynamics and

976 neurodegenerative disorders. Nature Reviews Neurology. Nature Publishing Group;
977 2015. pp. 11–24. doi:10.1038/nrneurol.2014.228
978 9. Schon EA, Dimauro S, Hirano M. Human mitochondrial DNA: Roles of inherited and
979 somatic mutations. Nature Reviews Genetics. 2012. pp. 878–890. doi:10.1038/nrg3275
980 10. Brown WM, George M, Wilson AC. Rapid evolution of animal mitochondrial DNA. Proc
981 Natl Acad Sci U S A. 1979;76: 1967–1971. doi:10.1073/pnas.76.4.1967
982 11. Konrad A, Thompson O, Waterston RH, Moerman DG, Keightley PD, Bergthorsson U, et
983 al. Mitochondrial mutation rate, spectrum and heteroplasmy in Caenorhabditis elegans
984 spontaneous mutation accumulation lines of differing population size. Mol Biol Evol.
985 Oxford University Press; 2017;34: 1319–1334. doi:10.1093/molbev/msx051
986 12. Denver DR, Morris K, Lynch M, Vassilieva LL, Thomas WK. High direct estimate of the
987 mutation rate in the mitochondrial genome of Caenorhabditis elegans. Science (80-).
988 2000;289: 2342–2344. doi:10.1126/science.289.5488.2342
989 13. Palozzi JM, Jeedigunta SP, Hurd TR. Mitochondrial DNA Purifying Selection in Mammals
990 and Invertebrates. Journal of Molecular Biology. Academic Press; 2018. pp. 4834–4848.
991 doi:10.1016/j.jmb.2018.10.019
992 14. Stewart JB, Freyer C, Elson JL, Larsson NG. Purifying selection of mtDNA and its
993 implications for understanding evolution and mitochondrial disease. Nature Reviews
994 Genetics. 2008. pp. 657–662. doi:10.1038/nrg2396
995 15. Twig G, Shirihai OS. The interplay between mitochondrial dynamics and mitophagy.
996 Antioxidants and Redox Signaling. 2011. pp. 1939–1951. doi:10.1089/ars.2010.3779
997 16. Busch KB, Kowald A, Spelbrink JN. Quality matters: How does mitochondrial network

998 dynamics and quality control impact on mtDNA integrity? Philosophical Transactions of
999 the Royal Society B: Biological Sciences. Royal Society of London; 2014.
1000 doi:10.1098/rstb.2013.0442
1001 17. Ni HM, Williams JA, Ding WX. Mitochondrial dynamics and mitochondrial quality control.
1002 Redox Biology. Elsevier B.V.; 2015. pp. 6–13. doi:10.1016/j.redox.2014.11.006
1003 18. Ashrafi G, Schwarz TL. The pathways of mitophagy for quality control and clearance of
1004 mitochondria. Cell Death and Differentiation. 2013. pp. 31–42. doi:10.1038/cdd.2012.81
1005 19. Youle RJ, Narendra DP. Mechanisms of mitophagy. Nat Rev Mol Cell Biol. 2011;12: 9–14.
1006 doi:10.1038/nrm3028
1007 20. Tilokani L, Nagashima S, Paupe V, Prudent J. Mitochondrial dynamics: Overview of
1008 molecular mechanisms. Essays in Biochemistry. Portland Press Ltd; 2018. pp. 341–360.
1009 doi:10.1042/EBC20170104
1010 21. Hernando-Rodríguez B, Artal-Sanz M. Mitochondrial Quality Control Mechanisms and the
1011 PHB (Prohibitin) Complex. Cells. MDPI AG; 2018;7: 238. doi:10.3390/cells7120238
1012 22. Sté phane Rolland AG, Schneid S, Schwarz M, Mokranjac D, Lambie E, Conradt B.
1013 Compromised Mitochondrial Protein Import Acts as a Signal for UPR mt. Cell Rep.
1014 2019;28: 1659–1669. doi:10.1016/j.celrep.2019.07.049
1015 23. Münch C. The different axes of the mammalian mitochondrial unfolded protein response.
1016 BMC Biology. BioMed Central Ltd.; 2018. doi:10.1186/s12915-018-0548-x
1017 24. Callegari S, Dennerlein S. Sensing the stress: A role for the UPR mt and UPR am in the
1018 quality control of mitochondria. Frontiers in Cell and Developmental Biology. Frontiers
1019 Media S.A.; 2018. doi:10.3389/fcell.2018.00031

1020 25. Gitschlag BL, Kirby CS, Samuels DC, Gangula RD, Mallal SA, Patel MR. Homeostatic
1021 Responses Regulate Selfish Mitochondrial Genome Dynamics in C. elegans. Cell Metab.
1022 Cell Press; 2016;24: 91–103. doi:10.1016/j.cmet.2016.06.008
1023 26. Nargund AM, Pellegrino MW, Fiorese CJ, Baker BM, Haynes CM. Mitochondrial import
1024 efficiency of ATFS-1 regulates mitochondrial UPR activation. Science (80-). American
1025 Association for the Advancement of Science; 2012;337: 587–590.
1026 doi:10.1126/science.1223560
1027 27. Lin YF, Schulz AM, Pellegrino MW, Lu Y, Shaham S, Haynes CM. Maintenance and
1028 propagation of a deleterious mitochondrial genome by the mitochondrial unfolded
1029 protein response. Nature. Nature Publishing Group; 2016;533: 416–419.
1030 doi:10.1038/nature17989
1031 28. Murphy CT, Hu PJ. Insulin/insulin-like growth factor signaling in C. elegans [Internet].
1032 WormBook : the online review of C. elegans biology. 2013. pp. 1–43.
1033 doi:10.1895/wormbook.1.164.1
1034 29. Haroon S, Li A, Weinert JL, Fritsch C, Ericson NG, Alexander-Floyd J, et al. Multiple
1035 Molecular Mechanisms Rescue mtDNA Disease in C. elegans. Cell Rep. Elsevier B.V.;
1036 2018;22: 3115–3125. doi:10.1016/j.celrep.2018.02.099
1037 30. Lord CEN, Gunawardena AHLAN. Programmed cell death in C. elegans, mammals and
1038 plants. European Journal of Cell Biology. 2012. pp. 603–613.
1039 doi:10.1016/j.ejcb.2012.02.002
1040 31. Jeong SY, Seol DW. The role of mitochondria in apoptosis. Journal of Biochemistry and
1041 Molecular Biology. 2008. pp. 11–22. doi:10.5483/bmbrep.2008.41.1.011

1042 32. Estaquier J, Vallette F, Vayssiere JL, Mignotte B. The mitochondrial pathways of
1043 apoptosis. Adv Exp Med Biol. 2012;942: 157–183. doi:10.1007/978-94-007-2869-1_7
1044 33. Bhola PD, Letai A. Mitochondria-Judges and Executioners of Cell Death Sentences.
1045 Molecular Cell. Cell Press; 2016. pp. 695–704. doi:10.1016/j.molcel.2016.02.019
1046 34. Tower J. Programmed cell death in aging. Ageing Research Reviews. Elsevier Ireland Ltd;
1047 2015. pp. 90–100. doi:10.1016/j.arr.2015.04.002
1048 35. Larsson N-G. Somatic Mitochondrial DNA Mutations in Mammalian Aging. Annu Rev
1049 Biochem. Annual Reviews; 2010;79: 683–706. doi:10.1146/annurev-biochem-060408-
1050 093701
1051 36. Payne BAI, Chinnery PF. Mitochondrial dysfunction in aging: Much progress but many
1052 unresolved questions. Biochim Biophys Acta. 2015;1847: 1347–53.
1053 doi:10.1016/j.bbabio.2015.05.022
1054 37. Kauppila TES, Kauppila JHK, Larsson NG. Mammalian Mitochondria and Aging: An
1055 Update. Cell Metabolism. Cell Press; 2017. pp. 57–71. doi:10.1016/j.cmet.2016.09.017
1056 38. Conradt B, Wu YC, Xue D. Programmed cell death during Caenorhabditis elegans
1057 development. Genetics. Genetics; 2016;203: 1533–1562.
1058 doi:10.1534/genetics.115.186247
1059 39. Gumienny TL, Lambie E, Hartwieg E, Horvitz HR, Hengartner MO. Genetic control of
1060 programmed cell death in the Caenorhabditis elegans hermaphrodite germline.
1061 Development. 1999;126: 1011–1022. doi:10.5167/uzh-1041
1062 40. Baum JS, St. George JP, McCall K. Programmed cell death in the germline. Seminars in
1063 Cell and Developmental Biology. Elsevier Ltd; 2005. pp. 245–259.

1064 doi:10.1016/j.semcdb.2004.12.008

1065 41. Jaramillo-Lambert A, Ellefson M, Villeneuve AM, Engebrecht JA. Differential timing of S
1066 phases, X chromosome replication, and meiotic prophase in the C. elegans germ line. Dev
1067 Biol. Academic Press Inc.; 2007;308: 206–221. doi:10.1016/j.ydbio.2007.05.019

1068 42. Hafner A, Bulyk ML, Jambhekar A, Lahav G. The multiple mechanisms that regulate p53
1069 activity and cell fate. Nature Reviews Molecular Cell Biology. Nature Publishing Group;
1070 2019. pp. 199–210. doi:10.1038/s41580-019-0110-x

1071 43. Derry WB, Putzke AP, Rothman JH. Caenorhabditis elegans p53: Role in apoptosis,
1072 meiosis, and stress resistance. Science (80-). 2001;294: 591–595.
1073 doi:10.1126/science.1065486

1074 44. Huang W, Jiang T, Choi W, Qi S, Pang Y, Hu Q, et al. Mechanistic insights into CED-4-
1075 mediated activation of CED-3. Genes Dev. Genes Dev; 2013;27: 2039–2048.
1076 doi:10.1101/GAD.224428.113

1077 45. Seshagiri S, Miller LK. Caenorhabditis elegans CED-4 stimulates CED-3 processing and
1078 CED-3-induced. Curr Biol. Cell Press; 1997;7: 455–460. doi:10.1016/S0960-
1079 9822(06)00216-8

1080 46. Tsang WY, Lemire BD. Stable heteroplasmy but differential inheritance of a large
1081 mitochondrial DNA deletion in nematodes. Biochem Cell Biol. 2002;80: 645–654.
1082 doi:10.1139/o02-135

1083 47. Lemire B. Mitochondrial genetics. WormBook. 2005; doi:10.1895/wormbook.1.25.1

1084 48. Van Der Bliek AM, Sedensky MM, Morgan PG. Cell biology of the mitochondrion.
1085 Genetics. Genetics Society of America; 2017;207: 843–871.

1086 doi:10.1534/genetics.117.300262

1087 49. Sousa JS, D'Imprima E, Vonck J. Mitochondrial respiratory chain complexes. Subcellular
1088 Biochemistry. Springer New York; 2018. pp. 167–227. doi:10.1007/978-981-10-7757-9_7

1089 50. Baradaran R, Berrisford JM, Minhas GS, Sazanov LA. Crystal structure of the entire
1090 respiratory complex i. Nature. Nature; 2013;494: 443–448. doi:10.1038/nature11871

1091 51. Song Z, Laleve A, Vallières C, McGeehan JE, Lloyd RE, Meunier B. Human Mitochondrial
1092 Cytochrome b Variants Studied in Yeast: Not All Are Silent Polymorphisms. Hum Mutat.
1093 John Wiley and Sons Inc.; 2016;37: 933–941. doi:10.1002/humu.23024

1094 52. Gartner A, Boag PR, Blackwell TK. Germline survival and apoptosis. WormBook : the
1095 online review of C. elegans biology. 2008. pp. 1–20. doi:10.1895/wormbook.1.145.1

1096 53. Cohen GM. Caspases: The executioners of apoptosis. Biochemical Journal. Portland Press
1097 Ltd; 1997. pp. 1–16. doi:10.1042/bj3260001

1098 54. Shaham S, Reddien PW, Davies B, Horvitz HR. Mutational Analysis of the Caenorhabditis
1099 elegans Cell-Death Gene ced-3. Genetics. 1999;153.

1100 55. Jeong PY, Kumar A, Joshi PM, Rothman JH. Intertwined Functions of Separase and
1101 Caspase in Cell Division and Programmed Cell Death. Sci Rep. Nature Research; 2020;10.
1102 doi:10.1038/s41598-020-63081-w

1103 56. Denning DP, Hatch V, Horvitz HR. Both the Caspase CSP-1 and a Caspase-Independent
1104 Pathway Promote Programmed Cell Death in Parallel to the Canonical Pathway for
1105 Apoptosis in Caenorhabditis elegans. PLoS Genet. 2013;9.
1106 doi:10.1371/journal.pgen.1003341

1107 57. Shaham S. Identification of multiple Caenorhabditis elegans caspases and their potential

1108 roles in proteolytic cascades. J Biol Chem. 1998;273: 35109–35117.
1109 doi:10.1074/jbc.273.52.35109
1110 58. King SD, Gray CF, Song L, Nechushtai R, Gumienny TL, Mittler R, et al. The cisd gene
1111 family regulates physiological germline apoptosis through ced-13 and the canonical cell
1112 death pathway in Caenorhabditis elegans. Cell Death Differ. Nature Publishing Group;
1113 2019;26: 162–178. doi:10.1038/s41418-018-0108-5
1114 59. Schumacher B, Schertel C, Wittenburg N, Tuck S, Mitani S, Gartner A, et al. C. elegans
1115 ced-13 can promote apoptosis and is induced in response to DNA damage. Cell Death
1116 Differ. Nature Publishing Group; 2005;12: 153–161. doi:10.1038/sj.cdd.4401539
1117 60. Fairlie WD, Perugini MA, Kvansakul M, Chen L, Huang DCS, Colman PM. CED-4 forms a 2 :
1118 2 heterotetrameric complex with CED-9 until specifically displaced by EGL-1 or CED-13.
1119 Cell Death Differ. 2006;13: 426–434. doi:10.1038/sj.cdd.4401762
1120 61. Conradt B, Xue D. Programmed cell death. WormBook : the online review of C. elegans
1121 biology. 2005. pp. 1–13. doi:10.1895/wormbook.1.32.1
1122 62. Wu D, Chai Y, Zhu Z, Li W, Ou G, Li W. CED-10-WASP-Arp2/3 signaling axis regulates
1123 apoptotic cell corpse engulfment in C. elegans. Dev Biol. Academic Press Inc.; 2017;428:
1124 215–223. doi:10.1016/j.ydbio.2017.06.005
1125 63. Kinchen JM, Cabello J, Kilngele D, Wong K, Felchtinger R, Schnabel H, et al. Two pathways
1126 converge at CED-10 to mediate actin rearrangement and corpse removal in C. elegans.
1127 Nature. 2005;434: 93–99. doi:10.1038/nature03263
1128 64. Hochreiter-Hufford A, Ravichandran KS. Clearing the dead: Apoptotic cell sensing,
1129 recognition, engulfment, and digestion. Cold Spring Harb Perspect Biol. 2013;5.

1130 doi:10.1101/cshperspect.a008748

1131 65. Wang X, Yang C. Programmed cell death and clearance of cell corpses in Caenorhabditis
1132 elegans. Cellular and Molecular Life Sciences. Birkhauser Verlag AG; 2016. pp. 2221–
1133 2236. doi:10.1007/s00018-016-2196-z

1134 66. Reddien PW, Horvitz HR. THE ENGULFMENT PROCESS OF PROGRAMMED CELL DEATH IN
1135 *CAENORHABDITIS ELEGANS*. Annu Rev Cell Dev Biol. Annual Reviews; 2004;20: 193–221.
1136 doi:10.1146/annurev.cellbio.20.022003.114619

1137 67. Hoeppner DJ, Hengartner MO, Schnabel R. Engulfment genes cooperate with ced-3 to
1138 promote cell death in Caenorhabditis elegans. Nature. Nature Publishing Group;
1139 2001;412: 202–206. doi:10.1038/35084103

1140 68. Geng X, Zhou QH, Kage-Nakadai E, Shi Y, Yan N, Mitani S, et al. Caenorhabditis elegans
1141 caspase homolog CSP-2 inhibits CED-3 autoactivation and apoptosis in germ cells. Cell
1142 Death Differ. 2009;16: 1385–1394. doi:10.1038/cdd.2009.88

1143 69. Yang X, Chang HY, Baltimore D. Essential role of CED-4 oligomerization in CED-3
1144 activation and apoptosis. Science (80-). American Association for the Advancement of
1145 Science; 1998;281: 1355–1357. doi:10.1126/science.281.5381.1355

1146 70. Parsons MJ, Green DR. Mitochondria in cell death. Essays Biochem. 2010;47: 99–114.
1147 doi:10.1042/BSE0470099

1148 71. Harman D. Free radical theory of aging. Mutat Res. 1992;275: 257–266.
1149 doi:10.1016/0921-8734(92)90030-S

1150 72. HARMAN D. Aging: a theory based on free radical and radiation chemistry. J Gerontol.
1151 1956;11: 298–300. doi:10.1093/geronj/11.3.298

1152 73. Szczepanowska K, Trifunovic A. Origins of mtDNA mutations in ageing. Essays in
1153 Biochemistry. Portland Press Ltd; 2017. pp. 325–337. doi:10.1042/EBC20160090
1154 74. Bratic A, Larsson N-G. The role of mitochondria in aging. J Clin Invest. 2013;123: 951–957.
1155 doi:10.1172/JCI64125
1156 75. Ziegler D V., Wiley CD, Velarde MC. Mitochondrial effectors of cellular senescence:
1157 Beyond the free radical theory of aging. Aging Cell. Blackwell Publishing Ltd; 2015. pp. 1–
1158 7. doi:10.1111/acel.12287
1159 76. Kimble J, Crittenden SL. Germline proliferation and its control. WormBook : the online
1160 review of C. elegans biology. 2005. pp. 1–14. doi:10.1895/wormbook.1.13.1
1161 77. Yoon DS, Alfhili MA, Friend K, Lee MH. MPK-1/ERK regulatory network controls the
1162 number of sperm by regulating timing of sperm-oocyte switch in C. elegans germline.
1163 Biochem Biophys Res Commun. Elsevier B.V.; 2017;491: 1077–1082.
1164 doi:10.1016/j.bbrc.2017.08.014
1165 78. Angeles-Albores D, Leighton DHW, Tsou T, Khaw TH, Antoshechkin I, Sternberg PW. The
1166 Caenorhabditis elegans female-like state: Decoupling the transcriptomic effects of aging
1167 and sperm status. G3 Genes, Genomes, Genet. Genetics Society of America; 2017;7:
1168 2969–2977. doi:10.1534/g3.117.300080
1169 79. Kujoth CC, Hiona A, Pugh TD, Someya S, Panzer K, Wohlgemuth SE, et al. Medicine:
1170 Mitochondrial DNA mutations, oxidative stress, and apoptosis in mammalian aging.
1171 Science (80-). American Association for the Advancement of Science; 2005;309: 481–
1172 484. doi:10.1126/science.1112125
1173 80. Beanan MJ, Strome S. Characterization of a germ-line proliferation mutation in C.

1174 elegans. Development. 1992;116.

1175 81. Barton MK, Schedl TB, Kimble J. Gain-of-function mutations of fem-3, a sex-
1176 determination gene in Caenorhabditis elegans. Genetics. 1987;115: 107–119.

1177 82. Bartke A. Insulin and aging. Cell Cycle. Taylor and Francis Inc.; 2008. pp. 3338–3343.
1178 doi:10.4161/cc.7.21.7012

1179 83. Anisimov VN, Bartke A. The key role of growth hormone-insulin-IGF-1 signaling in aging
1180 and cancer. Critical Reviews in Oncology/Hematology. 2013. pp. 201–223.
1181 doi:10.1016/j.critrevonc.2013.01.005

1182 84. Piper MDW, Selman C, McElwee JJ, Partridge L. Separating cause from effect: how does
1183 insulin/IGF signalling control lifespan in worms, flies and mice? J Intern Med. John Wiley
1184 & Sons, Ltd; 2008;263: 179–191. doi:10.1111/J.1365-2796.2007.01906.X

1185 85. Kenyon C, Chang J, Gensch E, Rudner A, Tabtiang R. A C. elegans mutant that lives twice
1186 as long as wild type. Nature. 1993;366: 461–464. doi:10.1038/366461a0

1187 86. Tatar M, Kopelman A, Epstein D, Tu M-P, Yin C-M, Garofalo RS. A Mutant Drosophila
1188 Insulin Receptor Homolog That Extends Life-Span and Impairs Neuroendocrine Function.
1189 Science (80-). American Association for the Advancement of Science; 2001;292: 107–
1190 110. doi:10.1126/SCIENCE.1057987

1191 87. Blüher M, Kahn BB, Kahn CR. Extended Longevity in Mice Lacking the Insulin Receptor in
1192 Adipose Tissue. Science (80-). American Association for the Advancement of Science;
1193 2003;299: 572–574. doi:10.1126/SCIENCE.1078223

1194 88. Gitschlag BL, Tate AT, Patel MR. Nutrient status shapes selfish mitochondrial genome
1195 dynamics across different levels of selection. Elife. eLife Sciences Publications Ltd;

1196 2020;9: 1–27. doi:10.7554/ELIFE.56686

1197 89. Apfeld J, O'Connor G, McDonagh T, DiStefano PS, Curtis R. The AMP-activated protein
1198 kinase AAK-2 links energy levels and insulin-like signals to lifespan in C. elegans. Genes
1199 Dev. Cold Spring Harbor Laboratory Press; 2004;18: 3004–3009.
1200 doi:10.1101/gad.1255404

1201 90. Miyadera H, Kano K, Miyoshi H, Ishii N, Hekimi S, Kita K. Quinones in long-lived clk-1
1202 mutants of Caenorhabditis elegans. FEBS Lett. No longer published by Elsevier; 2002;512:
1203 33–37. doi:10.1016/S0014-5793(02)02282-2

1204 91. Miyadera H, Amino H, Hiraishi A, Taka H, Murayama K, Miyoshi H, et al. Altered Quinone
1205 Biosynthesis in the Long-lived clk-1Mutants of Caenorhabditis elegans. J Biol Chem.
1206 Elsevier; 2001;276: 7713–7716. doi:10.1074/JBC.C000889200

1207 92. Kirby CS, Patel MR. Elevated mitochondrial DNA copy number found in ubiquinone-
1208 deficient clk-1 mutants is not rescued by ubiquinone precursor 2-4-dihydroxybenzoate.
1209 Mitochondrion. Elsevier B.V.; 2021;58: 38–48. doi:10.1016/j.mito.2021.02.001

1210 93. Charmpilas N, Tavernarakis N. Mitochondrial maturation drives germline stem cell
1211 differentiation in Caenorhabditis elegans. Cell Death Differ. Springer Nature; 2020;27:
1212 601–617. doi:10.1038/s41418-019-0375-9

1213 94. Folmes CDL, Ma H, Mitalipov S, Terzic A. Mitochondria in pluripotent stem cells:
1214 Stemness regulators and disease targets. Current Opinion in Genetics and Development.
1215 Elsevier Ltd; 2016. pp. 1–7. doi:10.1016/j.gde.2016.02.001

1216 95. Floros VI, Pyle A, DIetmann S, Wei W, Tang WWC, Irie N, et al. Segregation of
1217 mitochondrial DNA heteroplasmy through a developmental genetic bottleneck in human

1218 embryos. Nat Cell Biol. 2018; 144–151. doi:10.1038/s41556-017-0017-8

1219 96. Zhang H, Burr SP, Chinnery PF. The mitochondrial DNA genetic bottleneck: Inheritance
1220 and beyond. Essays in Biochemistry. Portland Press Ltd; 2018. pp. 225–234.
1221 doi:10.1042/EBC20170096

1222 97. Wai T, Teoli D, Shoubridge EA. The mitochondrial DNA genetic bottleneck results from
1223 replication of a subpopulation of genomes. Nat Genet. 2008; 1484–1488.
1224 doi:10.1038/ng.258

1225 98. Liau WS, Gonzalez-Serricchio AS, Deshommes C, Chin K, LaMunyon CW. A persistent
1226 mitochondrial deletion reduces fitness and sperm performance in heteroplasmic
1227 populations of C. elegans. BMC Genet. BioMed Central; 2007;8: 1–11. doi:10.1186/1471-
1228 2156-8-8

1229 99. Zhu Z, Han X, Wang Y, Liu W, Lu Y, Xu C, et al. Identification of Specific Nuclear Genetic
1230 Loci and Genes That Interact With the Mitochondrial Genome and Contribute to
1231 Fecundity in Caenorhabditis elegans. Front Genet. Frontiers; 2019;10: 28.
1232 doi:10.3389/fgene.2019.00028

1233 100. Levin L, Blumberg A, Barshad G, Mishmar D. Mito-nuclear co-evolution: The positive and
1234 negative sides of functional ancient mutations. Front Genet. Frontiers Media S.A.;
1235 2014;5: 448. doi:10.3389/fgene.2014.00448

1236 101. Paliwal S, Fiumera AC, Fiumera HL. Mitochondrial-nuclear epistasis contributes to
1237 phenotypic variation and coadaptation in natural isolates of saccharomyces cerevisiae.
1238 Genetics. Genetics Society of America; 2014;198: 1251–1265.
1239 doi:10.1534/genetics.114.168575

1240 102. Zhu CT, Ingelmo P, Rand DM. G×G×E for Lifespan in Drosophila: Mitochondrial, Nuclear,
1241 and Dietary Interactions that Modify Longevity. PLoS Genet. Public Library of Science;
1242 2014;10. doi:10.1371/journal.pgen.1004354
1243 103. Meiklejohn CD, Holmbeck MA, Siddiq MA, Abt DN, Rand DM, Montooth KL. An
1244 Incompatibility between a Mitochondrial tRNA and Its Nuclear-Encoded tRNA Synthetase
1245 Compromises Development and Fitness in Drosophila. PLoS Genet. Public Library of
1246 Science; 2013;9. doi:10.1371/journal.pgen.1003238
1247 104. Dingley SD, Polyak E, Ostrovsky J, Srinivasan S, Lee I, Rosenfeld AB, et al. Mitochondrial
1248 DNA Variant in COX1 Subunit Significantly Alters Energy Metabolism of Geographically
1249 Divergent Wild Isolates in Caenorhabditis elegans. J Mol Biol. 2014;426: 2199–2216.
1250 doi:10.1016/j.jmb.2014.02.009
1251 105. Yee C, Yang W, Hekimi S. The intrinsic apoptosis pathway mediates the pro-longevity
1252 response to mitochondrial ROS in C. elegans. Cell. PMC Canada manuscript submission;
1253 2014;157: 897. doi:10.1016/J.CELL.2014.02.055
1254 106. H H, C K. Signals from the reproductive system regulate the lifespan of C. elegans.
1255 Nature. Nature; 1999;399: 362–366. doi:10.1038/20694
1256 107. L D, CW A, S K. New insights into apoptosome structure and function. Cell Death Differ.
1257 Cell Death Differ; 2018;25: 1194–1208. doi:10.1038/S41418-017-0025-Z
1258 108. S Y, X Y, JM A, JE H, SJ L, CW A. The holo-apoptosome: activation of procaspase-9 and
1259 interactions with caspase-3. Structure. Structure; 2011;19: 1084–1096.
1260 doi:10.1016/J.STR.2011.07.001
1261 109. Zermati Y, Mouhamad S, Stergiou L, Besse B, Galluzzi L, Boehrer S, et al. Nonapoptotic

1262 Role for Apaf-1 in the DNA Damage Checkpoint. Mol Cell. Cell Press; 2007;28: 624–637.
1263 doi:10.1016/j.molcel.2007.09.030
1264 110. Ferraro E, Pesaresi MG, De Zio D, Cencioni MT, Gortat A, Cozzolino M, et al. Apaf1 plays a
1265 pro-survival role by regulating centrosome morphology and function. J Cell Sci. 2011;124:
1266 3450–3463. doi:10.1242/jcs.086298
1267 111. Liu WH, Lin YL, Wang JP, Liou W, Hou RF, Wu YC, et al. Restriction of vaccinia virus
1268 replication by a ced-3 and ced-4-dependent pathway in Caenorhabditis elegans. Proc
1269 Natl Acad Sci U S A. National Academy of Sciences; 2006;103: 4174–4179.
1270 doi:10.1073/pnas.0506442103
1271 112. Wang G, Sun L, Reina CP, Song I, Gabel C V., Driscoll M. CED-4 CARD domain residues can
1272 modulate non-apoptotic neuronal regeneration functions independently from apoptosis.
1273 Sci Rep. 2019;9: 13315. doi:10.1038/s41598-019-49633-9
1274 113. Chaudhary D, O'Rourke K, Chinnaiyan AM, Dixit VM. The Death Inhibitory Molecules CED-
1275 9 and CED-4L Use a Common Mechanism to Inhibit the CED-3 Death Protease. J Biol
1276 Chem. Elsevier; 1998;273: 17708–17712. doi:10.1074/JBC.273.28.17708
1277 114. Mack HID, Zhang P, Fonslow BR, Yates JR. The protein kinase MBK-1 contributes to
1278 lifespan extension in daf-2 mutant and germline-deficient Caenorhabditis elegans. Aging
1279 (Albany NY). Impact Journals LLC; 2017;9: 1414–1432. doi:10.18632/aging.101244
1280 115. Libina N, Berman JR, Kenyon C. Tissue-Specific Activities of C. elegans DAF-16 in the
1281 Regulation of Lifespan. Cell. Cell Press; 2003;115: 489–502. doi:10.1016/S0092-
1282 8674(03)00889-4
1283 116. Lapierre LR, Hansen M. Lessons from C. elegans: signaling pathways for longevity. Trends

1284 Endocrinol Metab. Elsevier Current Trends; 2012;23: 637–644.
1285 doi:10.1016/J.TEM.2012.07.007
1286 117. A A. Regulation of longevity by the reproductive system. Exp Gerontol. Exp Gerontol;
1287 2013;48: 596–602. doi:10.1016/J.EXGER.2012.09.009
1288 118. Branicky R, Bénard C, Hekimi S. clk-1, mitochondria, and physiological rates. BioEssays.
1289 2000. pp. 48–56. doi:10.1002/(SICI)1521-1878(200001)22:1<48::AID-BIES9>3.0.CO;2-F
1290 119. Hekimi S, Guarente L. Genetics and the specificity of the aging process. Science. 2003. pp.
1291 1351–1354. doi:10.1126/science.1082358
1292 120. Blackwell TK, Steinbaugh MJ, Hourihan JM, Ewald CY, Isik M. SKN-1/Nrf, stress responses,
1293 and aging in Caenorhabditis elegans. Free Radic Biol Med. Pergamon; 2015;88: 290–301.
1294 doi:10.1016/J.FREERADBIOMED.2015.06.008
1295 121. Youle RJ, Van Der Bliek AM. Mitochondrial fission, fusion, and stress. Science. American
1296 Association for the Advancement of Science; 2012. pp. 1062–1065.
1297 doi:10.1126/science.1219855
1298 122. Twig G, Elorza A, Molina AJA, Mohamed H, Wikstrom JD, Walzer G, et al. Fission and
1299 selective fusion govern mitochondrial segregation and elimination by autophagy. EMBO
1300 J. 2008;27: 433–446. doi:10.1038/sj.emboj.7601963
1301 123. Stiernagle T. Maintenance of C. elegans. WormBook : the online review of C. elegans
1302 biology. 2006. pp. 1–11. doi:10.1895/wormbook.1.101.1
1303 124. C. elegans Deletion Mutant Consortium. large-scale screening for targeted knockouts in
1304 the Caenorhabditis elegans genome. G3 (Bethesda). 2012;2: 1415–25.
1305 doi:10.1534/g3.112.003830

1306 125. Li H, Durbin R. Fast and accurate short read alignment with Burrows–Wheeler transform.
1307 Bioinformatics. Oxford Academic; 2009;25: 1754–1760.
1308 doi:10.1093/BIOINFORMATICS/BTP324
1309 126. Li H, Handsaker B, Wysoker A, Fennell T, Ruan J, Homer N, et al. The Sequence
1310 Alignment/Map format and SAMtools. Bioinformatics. Oxford Academic; 2009;25: 2078–
1311 2079. doi:10.1093/BIOINFORMATICS/BTP352
1312 127. Koboldt DC, Chen K, Wylie T, Larson DE, McLellan MD, Mardis ER, et al. VarScan: variant
1313 detection in massively parallel sequencing of individual and pooled samples.
1314 Bioinformatics. Oxford Academic; 2009;25: 2283–2285.
1315 doi:10.1093/BIOINFORMATICS/BTP373
1316
1317